WIRELESS DEVICES FOR MEDICAL APPLICATIONS

by

THERMPON ATIVANICHAYAPHONG

Presented to the Faculty of the Graduate School of

The University of Texas at Arlington in Partial Fulfillment

of the Requirements

for the Degree of

DOCTOR OF PHILOSOPHY

THE UNIVERSITY OF TEXAS AT ARLINGTON

December 2007

ACKNOWLEDGEMENTS

I would like to express my appreciation and thankfulness to my supervising professor Dr. Jung-Chih Chiao. This thesis could not have been written without his guidance and his enthusiasm. His support and encouragement throughout the thesis enlighten me to finish this work. I also would like to thank Dr. Yuan Bo Peng and Dr. Shou-Jiang Tang for their innovative ideas and hard work that help me finish the massive experiments.

My sincere appreciation also extends to Ji-Wei He, Christopher E Hagains, Lara A Kachlic for their kindly help in the animal facility and Dr. H.F. Tibbals, Dr. Stuart Spechler, Dr. William H. Cantrell for their professional suggestions. Furthermore, I would like to thank my parents, my brother and my sister for their endless love, carefulness during the thesis progress. I also want to thank Dr. Jonathan Bredow, Dr. Ronal L. Carter and Dr. W. Alan Davis to be my thesis committee.

A special thanks to all of my friends in UTA and all colleges in iMEMS group. It has been a long journey for my education in United States that I have never expected. I have earned a lot of technical knowledge as well as life experience.

This project is sponsored by the NSF, ECS Division, IHCS Program, Grant #ECS-0601229 and AFOSR Grant #FA-9550-06-0413.

November 21, 2007

ABSTRACT

WIRELESS DEVICES FOR MEDICAL APPLICATIONS

Publication No. _____

THERMPON ATIVANICHAYAPHONG, PhD.

The University of Texas at Arlington, 2007

Supervising Professor: Jung-Chih Chiao

The deployment of medical electronics in healthcare plays a significant role to overcome many problems in disease treatment and diagnosis. For advanced applications, wireless solutions are preferred. The wireless technologies offer a new dimension of therapy or diagnosis, when wires are often bulky, unsafe, uncomfortable or even impossible to be deployed in some circumstances. The wireless communication devices can be categorized into two groups, active and passive, depending on the power sources operating electronics. The active devices draw powers from a battery, while the others harvest powers from external or internal sources. In this work, two medical applications are studied for pain management and gastroesophageal reflux diagnosis using active and passive wireless approaches, respectively.

The pain management systems are based on neurostimulation and neurorecording principles. The system requires batteries in implants for wireless communication. The neurostimulation can significantly improve pain relief when used on carefully selected chronic pain patients. An integrated recording and stimulating system has been designed, developed and used in animal experiments. The system consists of miniature components to record neuronal signals from the spinal cord and to activate the stimulation in the brain wirelessly. The system is equipped with a feedback function and decision making capability to automatically activate the stimulation from the recorded signals. A wearable prototype was tested in anesthetized rats. The results show that, when suitable stimulation parameters are used, the brain stimulation inhibits neural responses which may cause pain.

For gastroesophageal reflux diagnosis, a new method of wirelessly detecting reflux in esophagus was proposed. Based on passive telemetry using inductive links, impedance of the refluxates can be determined remotely. The impedance variation can be determined from either amplitude or frequency changes of the detected signals. Planar coils integrated with electrodes on flexible substrates have been fabricated for amplitude detection. A circuitry connected with the sensing electrodes has been built for frequency detection. The devices are characterized in acid and non-acid solutions including the experiments in animals. Both techniques were used in implantable sensors without a battery to distinguish air, water and acid reflux wirelessly with a reader. The design methodology can also be applied to other sensors to monitor physiological conditions in human body.

TABLE OF CONTENTS

LIST OF ILLUSTRATIONS

LIST OF TABLES

CHAPTER 1

INTRODUCTION

1.1 Motivation

Less than a decade ago, wireless solutions were uncommonly used in medical fields because the devices could not meet one or more of critical requirements either in the performance, the reliability or the cost effectiveness of the medical instruments. However, the recent advances in wireless technology have stimulated enormous interest in using it in healthcare due to the unique advantages that cannot be achieved by any other means. The wireless approach offers another dimension for therapy or diagnosis when wires are often too bulky, unsafe, uncomfortable or even impossible to be employed in some circumstances.

One of the most promising applications in the near future that will highly rely on the wireless approach is medical devices for implant. The unwired technique enables the data link from the implant to the outside world. With the ability to communicate between the devices after the implant procedures, the doctors can explore the next level of medical treatments. The risk of infection, injury and malfunction caused by bulky wires will be eliminated by the wireless technology as well.

In general, the wireless features involve collecting the data from the inside organs and sending the command to control the implanted devices. These are

fundamental building blocks of any wireless equipment for medical applications. For this reason, it is beneficial for electrical engineers to apply wireless technology to improve the current medical treatments.

1.2 Proposed applications

One of the emerging applications for implanted devices is in the neural engineering field. In this area, many researchers spend a lot of effort either to extract the data generated from the neuron or to apply electrical signals to manipulate its behavior. A significant application of neural engineering is to dealing with pain. The need to reduce pain in an individual is great, especially for chronic pain. The neural engineering approach provides a low level treatment directly related to the feeling of pain. The research in this area includes neural signal recording to evaluate pain and neural stimulation to ease the pain. During the past few years, there have been stimulating devices for pain reduction. Like a peace maker, the currently available devices are implanted and cannot be adjusted after the implant procedures. The implanted stimulator that could be automatically reconfigurable will be beneficial. For this reason, a new design using a wireless approach to reconfigure the device to achieve the optimum performance was proposed. The device, called an integrative recording and stimulating system, is capable of monitoring the pain level and automatically stimulated neurons to moderate the pain.

Another promising application for an implant is to detect the abnormal operation inside the human body. A wireless sensor is therefore needed to monitor the internal organs. In this thesis, the diagnosis of gastro esophageal reflux disease (GERD)

which causes a lot of people experience heart burn is focused. GERD is a result of improper function of the esophagus. The current diagnosis of GERD still relies on catheter base sensors to monitor the reflux. Although a wireless pH sensor has been available recently, it can only detect acid reflux and has a short battery life. We thus propose a wireless impedance sensor implanted in esophagus that can detect both acid and non-acid reflux. The batteryless design is suitable for long term monitoring.

In this thesis, two medical applications using wireless devices are proposed. Although the developed devices will be used in pain management and gastro esophageal reflux diagnosis, the fundamental operation of these devices, however, is a key component of many other applications that can benefit from the wireless approach as well.

1.3 Objectives and thesis organization

This thesis presents the detailed design of the devices and the experimental results. The system operation from the prototypes using animal test was demonstrated to provide the feasibility of using the same approaches to develop devices for humans. Specially, for each proposed application, the objective can be described as follows

Objective for the pain management application

- To provide new tools that can be used for study of pain signal processing
- The prototype will be used to evaluate the pain level from recorded neural signals and to stimulate neurons for pain relief
- The system should demonstrate the ability of the feedback loop to activate the stimulation when the pain level detected from the neuron reaches certain thresholds

- The prototype should be small enough to carried by a rat for animal test
- The fundamental operation of recording, stimulating and feedback loop control would be used in other applications of neural engineering

Objective for esophageal reflux diagnosis application

- To demonstrate the feasibility of using new techniques to reliably detect acid and non acid reflux in the esophagus
- The prototype should be small enough to be implanted in the esophagus
- The system should be able to wirelessly monitor the reflux through animal tissue without the need of a battery
- The new technique of sensing could be used to detect other conditions in the human body

This thesis is divided into 9 chapters. Chapters 2-4 are dedicated to the pain management application. Chapters 5-8 will discuss the details for gastroesophageal reflux diagnosis. In chapter 2, the pain problems are introduced, how it originates and the approach to alleviate the pain. The design of the integrated recording and stimulating system will be explored in Chapter 3 starting from overall system, recording part, stimulating part, feedback loop and the functionality of the device. Chapter 4 demonstrates the system using the rats for in vivo testing. All the results will be discussed in this chapter as well.

For the other application, currently available tools are introduced to diagnose GERD along with the proposed approaches to detect the reflux in chapter 5. Chapter 6 discusses all aspects of the proposed amplitude detection technique including the design, fabrication processes and the experiments. Another technique using frequency detection which is considered to be a better approach is introduced in Chapter 7. This chapter also includes design architecture, device performance and test results in animals. The results are compared with a commercial available wireless pH sensor. In Chapter 8, an improved feature of the sensor is proposed by adding the pH sensor along with the impedance sensor that could be the ultimate solution for gastro esophageal reflux monitoring tools. All the work in the thesis will be concluded in chapter 9 with a direction for future work.

CHAPTER 2

INTRODUCTION TO AN INTEGRATED WIRELESS NEURAL STIMULATING AND RECORDING SYSTEM FOR PAIN MANAGEMENT

2.1 Motivation

Chronic pain is a significant national health problem. It is the most common reason individuals seek medical care, with 40 million medical visits annually, costing the American public more than $100 billion each year [2.1]. Several major approaches have been used to ease pain, including (a) medication, the most common route to relieve pain; (b) surgery to correct the pathological site; (c) physical rehabilitation; (d) alternative medicines; and (e) surgical implantation of neurostimulators as the last resort.

Neurostimulation of the spinal cord or primary motor cortex delivers low levels of electrical currents directly to nerve fibers or neurons to affect the neuronal membrane excitability, in turn to suppress pain signals by opening and closing of ion channels through releasing various kinds of neurotransmitters [2.2-2.5]. This form of therapy is attractive because it is selective for pain and has few side effects [2.6] compared to other approaches. Neurostimulation reduces or blocks a pain signal rather than eliminating it. Therapeutic studies have shown when used on carefully selected chronic pain patients, neurostimulation could significantly improve pain relief and reduce use of narcotic medications [2.7-2.10]. There are several advantages of direct stimulation of

the nervous system. First, it can be very effective for certain conditions with few side effects. Second, the implanted device can be controlled by patients or doctors with little risk of addiction or overdose. Third, the implant could be removed if it does not achieve the desired level of pain or symptom relief. Some neurostimulation therapies have been carried out in clinical treatments. However, only a small percent of patients received the procedures.

The currently available stimulators, however, are open-loop systems in which the doctors can only obtain the results for pain management from patients' verbal feedback. The stimulating signals are programmed during the installation of the devices and cannot be modified after the patients leave the hospital. Over time, the same stimulating configuration might not be effective because of possible resistance the neurons may develop or the changes in the condition of the electrode interface. The goal of this research is to develop a closed-loop system that can automatically provide the optimal pain relief signals based on the physiological responses recorded from the neurons associated with the pain. Wired connection of the neurorecorders and neurostimulators, inside one's body is not suitable for safe, long-term uses. Ultimately, the system could be implemented as a wireless implantable microsystem [2.11]. However, at this stage, our focus is on the studies of pain signal processing. A simple wireless device capable of both recording and stimulating is necessary for our studies on freely moving animals.

2.2 Background of pain mechanism and the action potential (AP)

Pain is a complicated mechanism involving many of our body activities which requires a lot of knowledge in biology, neurology and several other areas to understand. In this section, however, only a general background of the pain mechanism in a simple way necessary to understand the work in this thesis will be provided. More details can be found in [2.12]. The action potential (AP) is the signaling used to transmit information between neurons in the nervous systems. The AP is generated from ions flowing through cell membrane and can be measured using appropriate electrodes and equipment. The shape of an ideal AP is shown in Fig. 2.1.

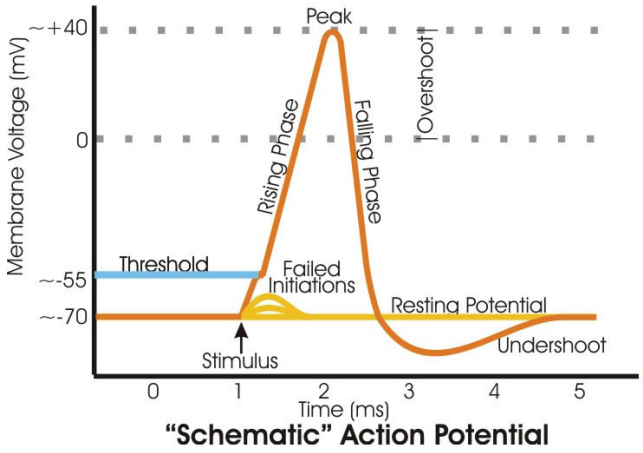

Figure 2.1 An action potential [2.14]

The AP can have an amplitude greater than 100 mVp-p in intracellular measurement. However for extracellular recording, where the recording electrode is outside the cell body, the signal amplitude could be attenuated to hundreds of micro

volts. The AP spike generally occupies a bandwidth between 500 Hz and 3 kHz [2.13]. For these reasons, electrodes, amplifiers and filters are required to record the APs.

In short, the feeling of pain can be explained roughly in a few steps. First, the sensory fibers convey the pain information to the spinal cord from the place where noxious stimuli are presented. The fibers terminate on neurons in the dorsal horn area of the spinal cord. Then APs are fired from the neurons and transmitted to the brain. This mechanism is a part of body's protection systems to notify the brain that there are noxious stimuli. It is at this point that we feel uncomfortable and response by trying to stop the pain if possible. The APs are used to transmit information, including pain. In other words, the techniques that can stop neurons from firing APs could potentially reduce the feeling of pain. One such technique is neural stimulation which is the approach in this thesis.

2.3 Proposed approach

In this thesis, a new way to evaluate the pain level from the number of APs recorded from a spinal cord dorsal horn neuron is proposed. More APs firing could indicate more pain. The pain can be reduced by applying electrical stimulation to specific brain area. The feedback system that can monitor the pain level and automatically apply the stimulation when the pain reaches a certain threshold is proposed. The recorded APs will be transmitted wireless and the electrical stimulation will be controlled wirelessly.

Although several wireless systems for animal tests have been developed, they are not perfectly suitable in our application either because of the large size [2.15], the

short transmission range [2.16], or the operating frequency that is not publicly allowed in United States [2.17-2.19]. Nevertheless, to our best knowledge, an integrated wireless recording and stimulating system that can provide an optimized signal feedback control of the electrical stimulation has yet been demonstrated.

To avoid the complexity of the wireless parts, commercial wireless modules were chosen. Using commercial off-the-shelf (COTS) for the wireless communications allows simple modification to achieve the best performance of existing wireless technologies as well. Some wireless modules have been deployed in both recording [2.20] and stimulating system [2.21] in freely moving rats. These modules had a communication range up to 300 m using the industrial, scientific and medical (ISM) band. We have combined both systems and modified to fit our application. Other than the wireless parts, the use of surface-mounted devices (SMDs) keeps the board size small after the integration. Our device was designed to be small and light weight to be carried by a rat.

The recording part transmits non-filtered signals to a receiver base station equipped with a 300-Hz to 10-kHz filter that extracts single neuron action potentials. The stimulating part delivers bipolar pulses with voltage levels up to ±18V. The numbers of pulses, pulse durations, pulse intervals and voltage levels are wirelessly adjustable from a computer using a Labview program. The system is also equipped with a feedback functions to assess the pain levels from the recorded signals and activate the stimulation with the optimum parameters that were obtained from the prior trials using the same device.

The experiments will be conducted in anesthetized rats as a validation study of the system, for further use in freely moving animals. The device is designed to be used with commercially available electrodes that are suitable for specific recording and stimulating areas.

2.4 Overall system

The recording section includes a receiver base station which records the amplified neuronal signals transmitted from the wireless transmitter on the rat (Fig. 2.2). The stimulating transmitter at the computer sends out commands to the receiver carried on the rat. The microcontroller reads the command and generates the desired stimulating signals. The telemetric device carried on the rat includes a wireless transmitter module, a wireless receiver module and a microcontroller module. It also includes other components for recording and stimulating circuitry. All parts were assembled on a PCB (printed circuit board) with a size of 2.5×5 cm^2 (Fig.2.3). The weight was 20g without batteries. Two 6-V lithium batteries (2CR1/3N, Sanyo) were chosen due to their small size. Each battery was used to operate each part separately to avoid interference. The battery has a capacity of 160mAh, allowing an experimental duration for more than 6 hours. The telemetric device can be put within a jacket to be worn by a freely moving rat. However, in this work, anesthetized rats were used to verify the device functionalities. The detailed operation and circuitry will be explained in Chapter 3.

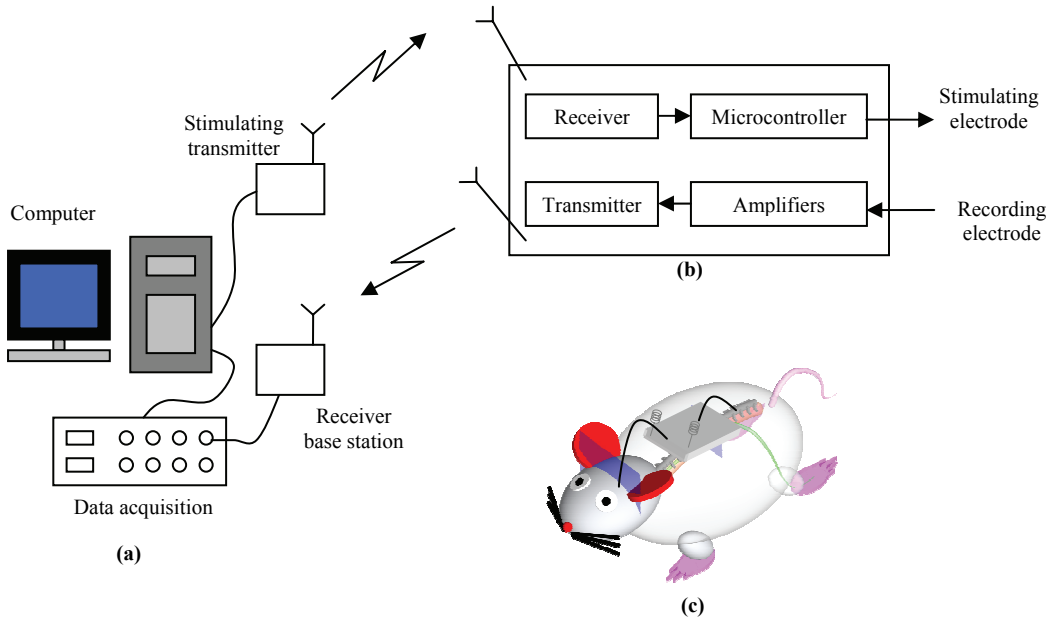

Figure 2.2 A combined wireless neuronal stimulating and recording system. (a) The receiver base station and stimulating transmitter. (b) The block diagram of the telemetric device. (c) The telemetric device is worn on the back of a rat.

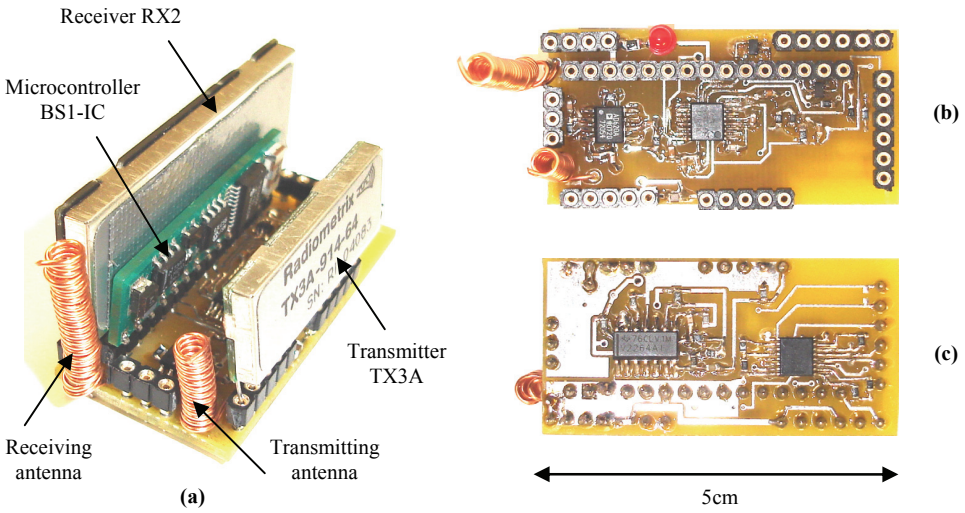

Figure 2.3 (a) The telemetric device without batteries. (b) Front side of the PCB without microcontroller and wireless modules. (c) Back side of the PCB.

CHAPTER 3

WIRELESS NEURAL RECORDER AND STIMULATOR WITH FEEDBACK LOOP

3.1 Wireless recorder

The wireless recording part consists of a transmitter board on the rat and a receiver base station. The transmitter board amplified and transmitted neuron signals to the receiver. The received signal was passed through a band-pass filter to extract the action potentials (APs). The signal was then input to a data acquisition unit connected to a computer (CED 1401Plus, Cambridge Electronic Design). The data was recorded and analyzed using a commercial software (Spike2, Cambridge Electronic Design).

3.1.1 Transmitter board

The circuit diagram of the transmitter board is shown in Fig. 3.1. A virtual ground was used to simulate positive and negative supplies for the operational amplifiers (op-amp) to amplify the APs that occupy both positive and negative cycles. It was made by a voltage divider using two of 100-kΩ resistors (R_9, R_{10}). The half 3-V is connected to an operational amplifier (op-amp) A4, as a buffer to maintain the voltage, which serves as the system ground of all amplifiers.

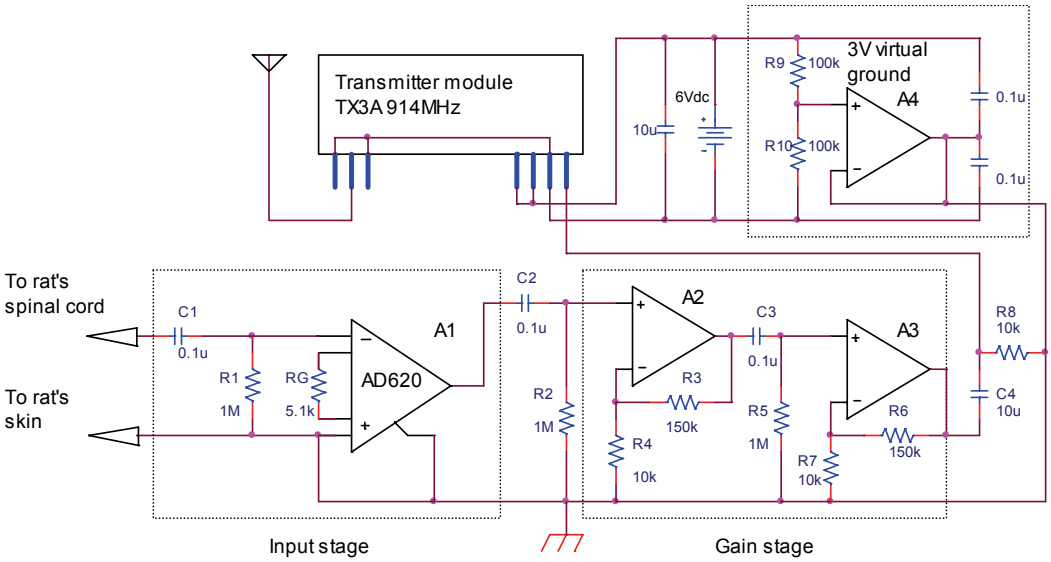

Figure 3.1 Circuit diagram of the transmitter board.

3.1.1.1 Input stage

Several constraints were imposed at the input stage due to the weak and noisy signals a neuron provides [3.1]. Three major parameters were considered. First, the amplitude of the extracellular AP is usually in the micro volt ranges. This low voltage is subjected to noise from electronic devices and nearby AC power lines. To eliminate the interference signals, a differential amplifier is necessary. The differential amplifier cancels the common mode noise presented at both the input and the reference electrodes. A high CMRR (common mode rejection ratio) of the amplifier is preferred. Second, due to the small sizes of the neurons, the recording electrode is usually thin creating a high impedance interface with the tissue. The amplifier at the input stage must have even higher input impedance to avoid attenuation of signals from the voltage

divider [3.2]. Third, unlike an ideal voltage source, the neuron provides very limited currents to the amplifier. The input bias current of the amplifier must be very low.

To achieve these requirements, one can connect three op-amps circuits are as an instrument amplifier [3.3]. However, to minimize the board space use, an integrated instrument amplifier (IA) in a single chip was considered. An integrated IA also consumes lower supply currents and provides an accurate gain. In our design, an integrated IA (AD620, Analog Device Inc.) was chosen. It has a CMRR of 80 dB, an input impedance of 1-GΩ and an input bias current of 2nA. The gain of AD620 can be programmed by a resistor R_G. A 5.1-kΩ for R_G is chosen, resulting in a gain of 10.7.

At the input, a high-pass filter C_1 (0.1μF) and R_1 (1MΩ) with a 1.6-Hz cut-off frequency was placed at the electrode to reduce the DC potential from the animal that might create artifacts. The 1-MΩ resistor also provides a current path to ground at the op-amp input. Without a resister, the charges accumulate and eventually saturate the op-amp [3.4]. Depending on the recording electrodes used, a low resistance value reduces the amplifier input impedance and attenuates the signals while a high resistance value increases the op-amp DC offset and saturates the amplifier [3.5]. The value of 1MΩ was achieved by experimental optimization.

3.1.1.2 Gain stage and transmitter module

After the pre-amp stage, the signal was amplified by a typical amplifier circuit. In our design, an op-amp (TLV2264, Texas Instrument) was used. This op-amp has a gain-bandwidth product of 670 kHz. Two stages of non-inverting amplifiers were added with an equal gain of 15. The total gain of the transmitter board was 2400. The

amplified signal was connected to a high-pass filter (C_4, R_8) to pull the signals from the virtual ground down to the 0-2.5V level which is the analog input range of the wireless transmitter module (TX3A, Radiometrix). The module operates in the 914MHz ISM band which is publicly allowed in the United States. It uses FM modulation and is capable of transmitting signals with a base band up to 35kHz within a range of 300m.

3.1.2 Receiver base station

A wireless receiver module (RX3A, Radiometrix) was used to receive the FM modulated data at 914MHz. The received signal includes low-frequency fluctuation, mainly at 60Hz coupling from AC power lines, and high-frequency noise. To eliminate the noises and extract the single neuron APs, a band-pass filter of 300Hz - 10kHz is used. The receiver circuit diagram is shown in Fig. 3.2. The frequency range can be easily modified following a reference filter design [3.6] to record other types of neuron activities (i.e., compound action potential at lower frequencies). Then the signal is amplified 10 times using an op-amp before it is fed to the CED1401Plus data acquisition unit.

3.2 Wireless stimulator

Our neurostimulator follows the design by Xu [3.7] that is capable of generating fixed ±5V bipolar pulses. In this design, the 433-MHz wireless module pair (TX2/RX2, Radiometrix) for communication was utilized. The transmitter TX2 was connected to an RS232 port in a computer, which sends out digital commands generated by a Labview program. The receiver module RX2 on the rat received the commands and feeds them to a microcontroller module (BS1-IC, Parallax Inc.) which has 8 input/output (I/O) pins.

The BS1-IC was programmed using the PBASIC language provided by the manufacturer. One I/O pin was used to receive the commands from the wireless module. Another pin was connected to an LED to indicate the working status during neurostimulation.

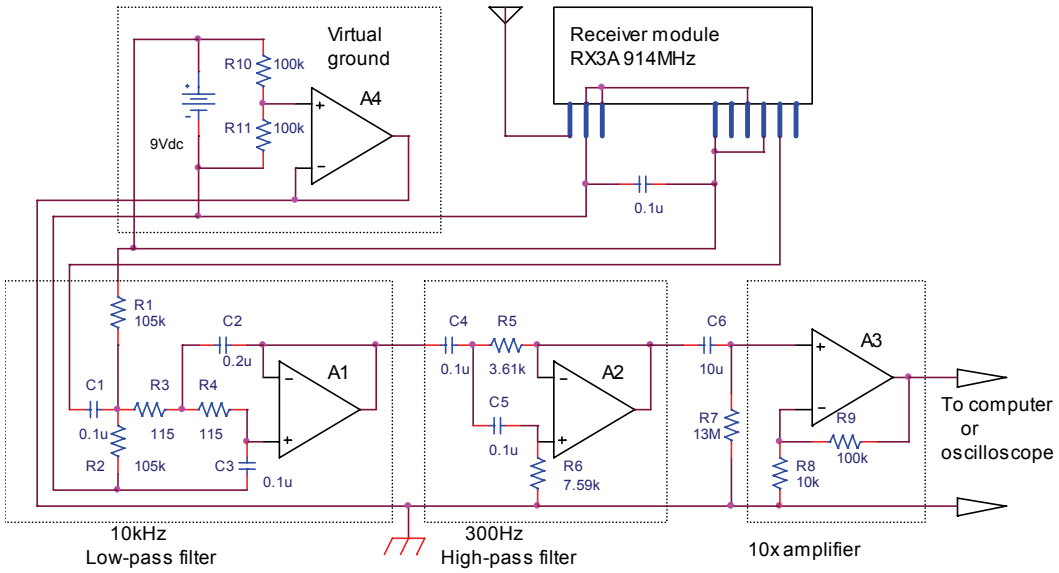

Figure 3.2 Circuit diagram of the receiver base station.

In this work, we have modified the stimulating system to generate bipolar pulses up to ±18V with adjustable voltage levels. The feature was achieved by using a charge pump (MAX202, Texas Instrument) to increase the voltage level and a multiplexer (CD4502B, Texas Instrument) to switch the voltage levels in 4 steps. The MAX202 was operated by a 5-V supply from BS1-IC, and the CD4502B was operated by a ±9V supply generated from the MAX202. The simplified circuit diagram is shown in Fig. 3.3. Two of the I/O pins from BS1-IC were used to create 0-5V stimulating pulses. The pulses were fed to the MAX202 resulting in ±9V signals. Each signal was fed to a series

of resistors (R_{X0}-R_{X4} and R_{Y0}-R_{Y4}) to tap out 4 different voltage levels, which can be arbitrarily adjusted by changing the resistance values. The tapped out voltages were sent to the multiplexer CD4502B into the X and Y channels. Three I/O pins of BS1-IC were used to control both switches of CD4502B to connect the outputs X and Y to any of the four tapped voltage levels. Three buffers (FDG6301, Fairchild Semiconductor) were used to translate the 5-V level from BS1-IC to the 9-V level required to control the CD4502B. The voltage of the bipolar pulses between the outputs X and Y therefore can be selected from 0V to ±18V. The stimulating pulse parameters including voltage levels, numbers of pulses, pulse durations, and pulse intervals are controlled wirelessly from a Labview program.

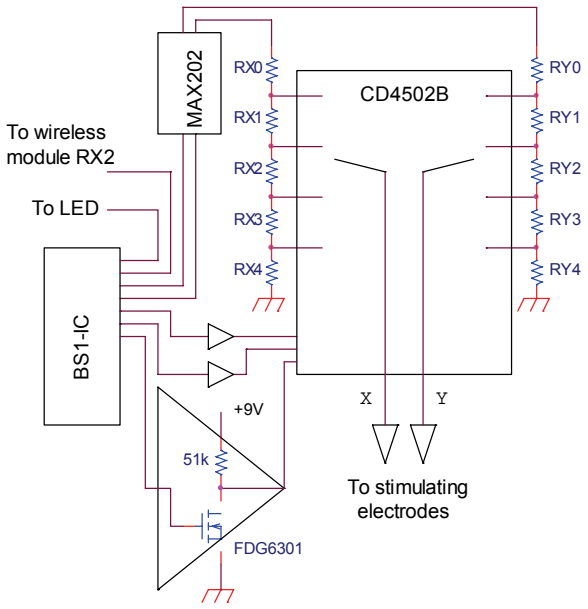

Figure 3.3 Simplified circuit diagram of the stimulating part.

3.4 Feedback systems

To activate the wirelessly controlled stimulation from the recorded neuron activities, we used a data acquisition (DAQ) module (USB-6008, National Instrument) to monitor the received wireless signals from the rat's spinal cord. The Labview program was used to estimate the rate of action potential (spikes/sec). This number represents the pain level when the mechanical stimulation is applied. The Labview program forms a feedback loop to activate the stimulator on the rat's brain when the rate is higher than specific threshold corresponding to high pain.

3.4.1 Rate estimation of APs

Although several commercial software programs such as Spike2 are available to calculate the rate of APs, they cannot be easily adapted to the Labview program to activate the stimulator. To demonstrate the feedback loop, it is more logical to use the same Labview program for both tasks. Nevertheless, the Spike2 was also used in parallel with the Labview to verify the accuracy of our system.

The DAQ module has a maximum sampling rate of 10ks/sec. which is enough to monitor the APs assuming that the bandwidth of the signal is less than 5kHz. Knowing that the APs are spikes and have much higher amplitude than that of the background noise, each AP can be counted when the measured signal is higher than certain threshold voltage. Two adjacent data points were averaged before they are compared to the threshold. This prevents the program from counting more than once from one AP. The threshold voltage, sampling rate and number of averaged data points can be adjusted for each experiment to get optimum accuracy. This simple estimation

technique, however, is subjected to errors from noise and artifacts in the measurement. Nevertheless, for this purpose, the relative response is focused, and it does not require very high accuracy.

The number of APs will be accumulated for a certain period of time, called the pain time slot. At the end of the slot, if the number of APs is more than the setting pain threshold level, the stimulation will be activated. The simplified operation of the feedback system is illustrated in Fig. 3.4, where x is the pain level threshold. The stimulation starts with dose#1 (the lowest dose with low voltage, less number of pulses, short duration and long interval) and if the pain level is still higher than the threshold more intense doses will be given gradually. When the pain reduces below the threshold, the stimulation will be stopped, and the loop begins again when the pain comes back.

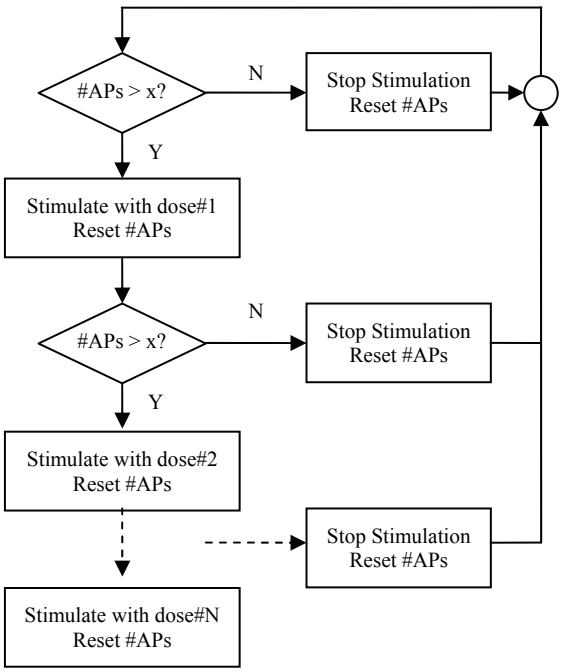

Figure 3.4 Flow diagram of a simple feedback algorithm.

More complex algorithm can be applied in the feedback loop using the same developed hardware. Ultimately, the doctor can run a pilot experiment to evaluate the efficiency of each stimulating parameter associated with the pain level. This database can be used in the decision making providing not only automatic stimulation, but also the most efficient way of pain relief. In this work, however, only a simple feedback loop will be used to demonstrate the feasibility of using the system for further studies. The Labview interface used for the feedback loop is shown in Fig. 3.5.

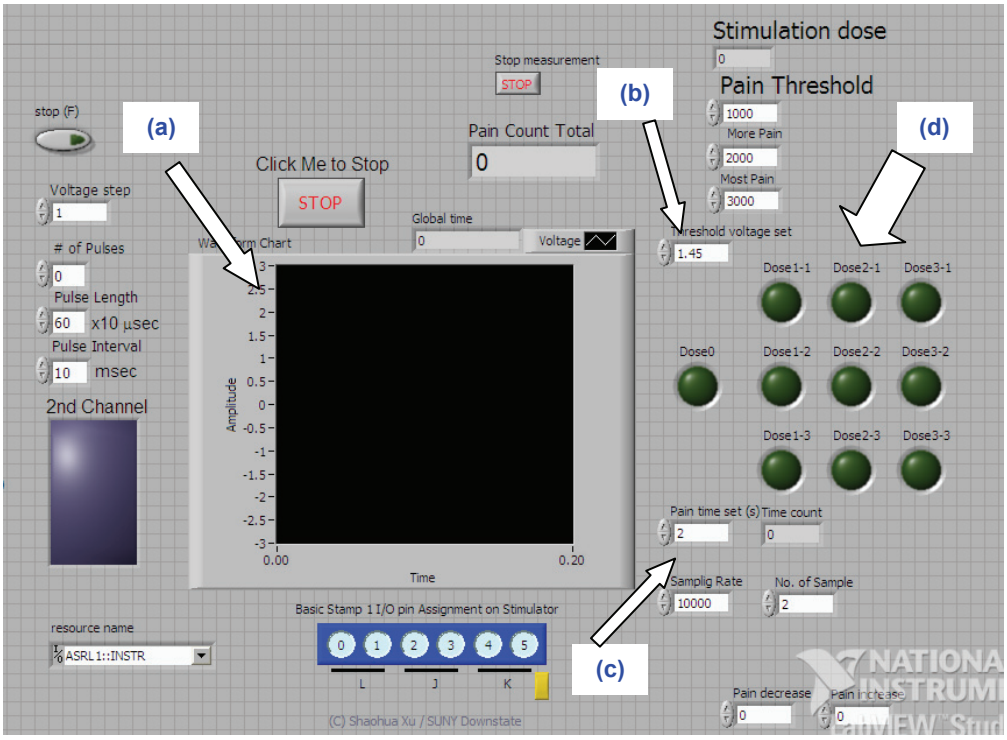

Figure 3.5 Labview interface for feedback loop system. (a) APs monitoring. (b) Threshold voltage. (c) Pain time slot. (d) Stimulation doses indicator.

CHAPTER 4

EXPERIMENTS

4.1 Experiment procedures

4.1.1 Animal preparation

Male Sprague-Dawley rats (300-350 g) are used in the experiments. All surgical procedures are approved by the University of Texas at Arlington Institutional Animal Care and Use Committee. The procedures are in accordance with the guidelines published by the Committee for Research and Ethical Issues of the International Association for Study of Pain [4.1]. Animals were anesthetized using sodium pentobarbital (50 mg/kg, i.p.). The spinal cord was exposed by performing a 3-4 cm laminectomy over the lumbosacral enlargement. A cannula was inserted in the trachea for artificial respiration if needed. The anesthesia was maintained by intravenous administration of sodium pentobarbital at a rate of 5mg/ml per hour. The pupil reflex was monitored periodically to ensure a proper depth of anesthesia. The spinal cord was immobilized in a stereotaxic frame and covered with mineral oil. The end tidal CO_2 was maintained at around 30 mmHg and the body temperature was maintained at 37˚C using a feedback controlled heating pad and a rectal thermal sensor probe.

4.1.2 Recording site and electrode

A tungsten microelectrode (10-12MΩ, FHC) was used for electrophysiological recordings in the rat's spinal cord dorsal horn where the nociceptive afferent fibers terminate [4.2]. The L5 and L6 regions were chosen because they respond to the rat's hind paw where the pain is applied by mechanical stimulation. The electrode was connected to the amplifiers on the wireless device. Single unit extracellular recordings were performed from the neurons that gave noticeable responses to the mechanical stimulation of the receptive fields in the plantar region of the hind paw. The data were recorded wirelessly using the CED 1401Plus and Spike2 software to extract the action potential signals.

4.1.3 Mechanical stimulation

Graded mechanical (brush, pressure, and pinch) stimulations were applied to the receptive fields in the hind paw to simulate pains. A camel hair brush was applied by moving over the receptive fields in a rhythmic fashion which was innocuous. Pressure was applied by a venous bulldog clamp (6 cm long, straight, serrated jaws) which was between innocuous and noxious. Pinch was applied by an arterial bulldog clamp (3 cm long, straight, serrated jaws) as a noxious stimulus. To analyze the pain level quantitatively, the applied force (F) as a function of displacement (x) of the clamp was measured. Fig. 4.1 shows the measured results. The graph follows the Hooke's Law, $F = kx$, where the slope, k, is the spring constant of the clamp. The slopes are 31.17 N/m for the pressure and 573 N/m for the pinch stimuli. As the clamp pressed onto the rat's feet within a 25-mm^2 area (A), and the clamp opened by 3 mm, the mechanical

pressures were 0.54 psi for the pressure stimulus and 9.35 psi for the pinch stimulus, respectively, calculated by $P = F/A = kx/A$.Each mechanical stimulus was applied once for 10s with an inter-stimulus interval of 20s. The pain response to each mechanical stimulus was measured as the number of action potentials per second that were recorded. Wide dynamic range (WDR) spinal dorsal horn neurons were selected for this study [4.3].

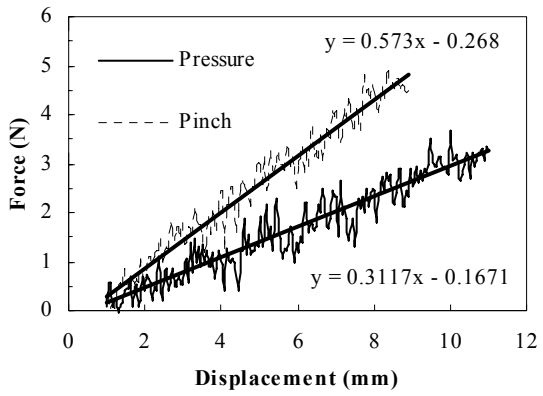

Figure 4.1 Measured forces as a function of displacement for the clips used for mechanical stimuli.

4.1.4 Stimulating site and electrode

Inhibition of spinal cord dorsal horn neuron activity has been demonstrated by stimulating midbrain periaqueductal gray (PAG) [4.4], as well as the anterior cingulate cortex (ACC) [4.5] using conventional wired systems. These results suggest that the PAG and ACC could be potential areas to stimulate for pain relief. The same brain areas were thus selected in this studies. After craniotomy, a bipolar stimulating electrode (*Science Products*) was placed in the PAG, 7.04mm caudal to bregma, 0.5mm lateral to the midline and 4.2mm deep from the brain surface (Fig. 4.2(a)). Another electrode was

placed in the ACC, 0.26mm caudal to bregma, 0.5mm lateral to the midline and 2.00mm dept (Fig. 4.2(b)). The electrode was selectively connected to the wireless device for bipolar stimulation depending on the desired stimulation area.

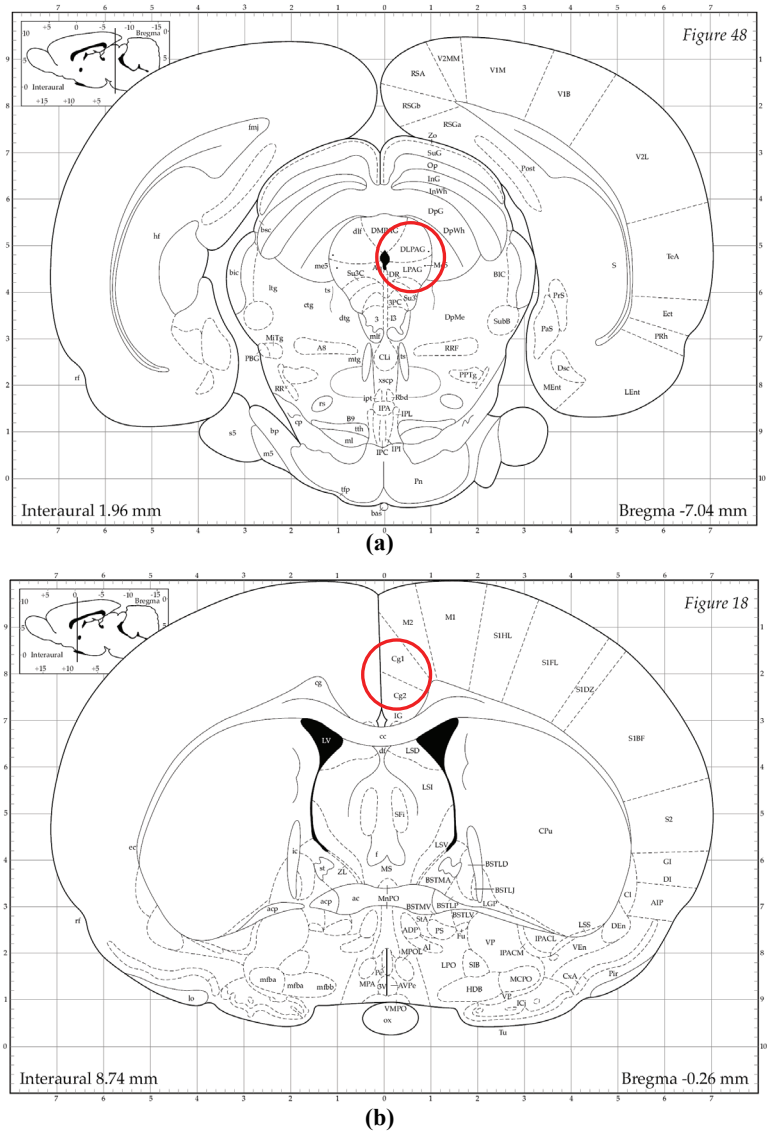

Figure 4.2 Stimulating site (a) PAG (b) ACC [4.6].

4.2 Device performance

The device was first tested using synthesized sinusoidal waveforms as input. Fig. 4.3 shows the output signals from the receiver base station.

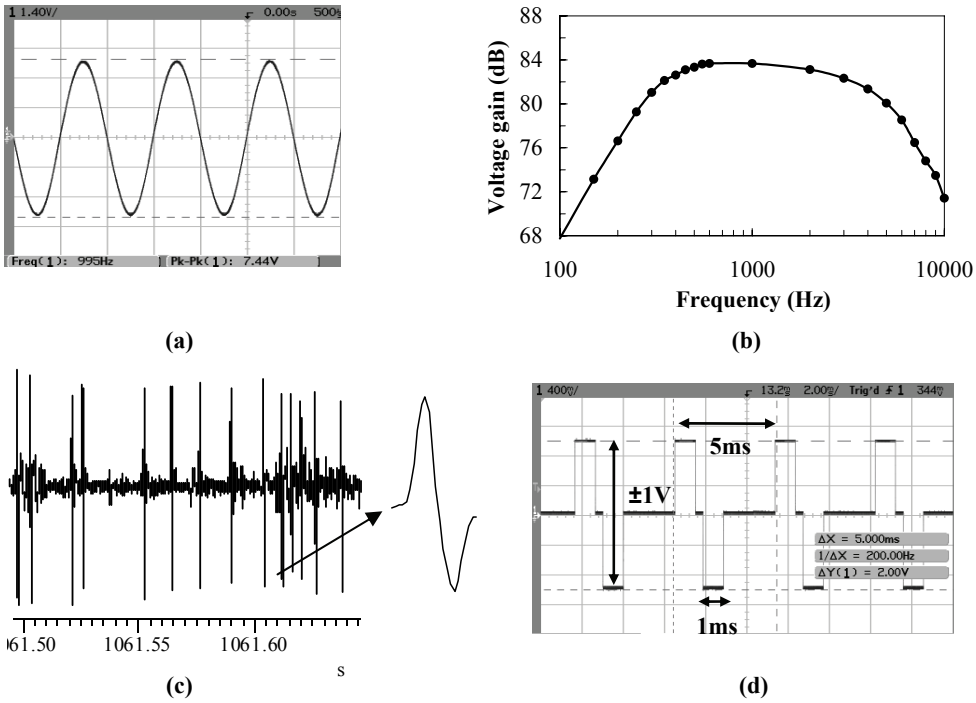

Figure 4.3(a) Recorded signals with an amplitude of 500µVp-p. (b) Frequency response of the system. (c) Recorded action potentials. (d) Neurostimulation pulses.

At 1 kHz, the 500 µVp-p signals were recorded with clear shapes (Fig. 4.3(a)) without visible distortion. The frequency response was measured from 100Hz to 10kHz with the 500 µVp-p input signals (Fig. 4.3(b)). The system gain at 1 kHz was around 15,000 or 84dB. The 3-dB bandwidth of the systems spanned from 300Hz to 4kHz. The device then was used with an anesthetized rat and Fig. 4.3(c) shows typical recorded action potentials (APs), with a single action potential waveform expanded as indicated

by the arrow. Four of bipolar pulses with a ±1V amplitude, a 1-ms duration and a 5-ms interval (or 200Hz) were generated from the device and recorded by an oscilloscope (Fig. 4.3(d)). The results show that the wireless system achieves the desired electrical performance.

4.3 Inhibitory effects on action potentials

To find out the relationship between the neuron responses and the given stimulating pulses, the Labview program was manually controlled to activate the stimulator on the rat during the recording. A series of pulses were given to the rat 4 times during the 10 second periods of the mechanical stimulation. Each stimulation lasted for 1 second. Various stimulating parameters including voltage levels, numbers of pulses, pulse durations, and pulse intervals were used to observe the inhibitory effects of the stimulation.

The single neuron recording examples, during the pressure stimuli on the rat's paw, with wirelessly controlled stimulation in the PAG and ACC areas are shown in Figs. 4.4 and 4.5, respectively. The lower trace (a) shows the recorded signals and the middle trace (b) indicates wireless command pulses that activate the neurostimulation which lasted for 1 second after the end of the command pulses. The upper trace (c) shows the rate histogram of APs (spikes/second) from the trace in (a). The stimulation parameters were 100 pulses, ±1.0V, 100Hz and 0.5-ms duration for PAG stimulation, and 50 pulses, ±16V, 50Hz and 0.5-ms duration for ACC stimulation.

From Fig. 4.4, when the pressure stimuli started, the rate of APs increased to 28 spikes/s (at 1273rd s-1274th s). The rate of APs reduced to 4 spikes/s when the first

stimulating pulses were applied (at 1274th s-1275th s). This corresponds to an inhibition percentage of 86%. After the stimulation ended, the rate of APs rose back to 11 spikes/s (at 1275th s-1276th s). When the second stimulating pulses were applied, the rate of APs decreased again achieving an inhibition of 55%.The similarly repeating cycles continued with the third and fourth stimulation, with inhibition of 80% and 100%, until the pressure stimuli were released after 10 seconds. The same phenomenon was also observed for ACC stimulation. The AP rate reduced when the wireless stimulating pulses were applied. In Figs. 4.4 and 4.5, the arrows indicate the inhibition percentages compared with 1 second period earlier when no neurostimulation is applied. From our results, with specific stimulating parameters, it seems possible to achieve inhibition of near 100% as the neuron stops firing during the stimulation. Another observation was that the ACC stimulation required a much higher voltage than that in the PAG case to achieve similar results. This high voltage introduced stimulation artifacts coupling through both air medium and the rat skin from the brain to the spinal cord [4.7]. It was possible to reduce the signals using aluminum foil grounding wrapped around the cables and the rat skin between the two electrodes.

Several experiments with various stimulating parameters were conducted under brush, pressure and pinch stimuli. We found that the inhibition highly depends on the stimulation parameters. The results vary with rats and recorded neurons as well. With this wireless device, combinations of stimulating parameters can be given in order to achieve optimal results.

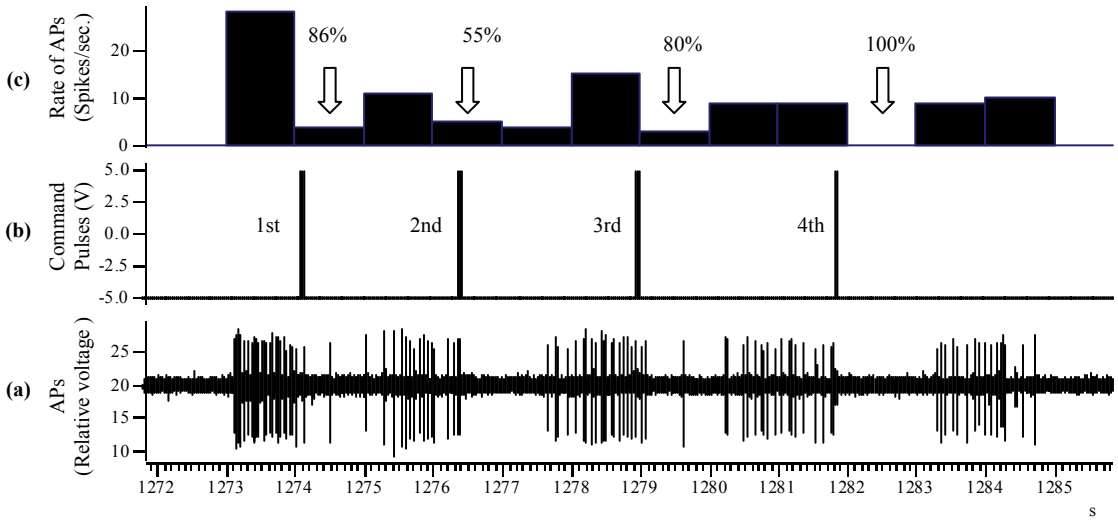

Figure 4.4 Inhibition effects with wireless PAG stimulation (Rat No. RT071207, cell No.6-4). (a) Rate of action potentials. (b) Command pulses of stimulation with 100 pulses, ±1.0V, 100Hz and 0.5-ms duration. (c) Recorded action potentials.

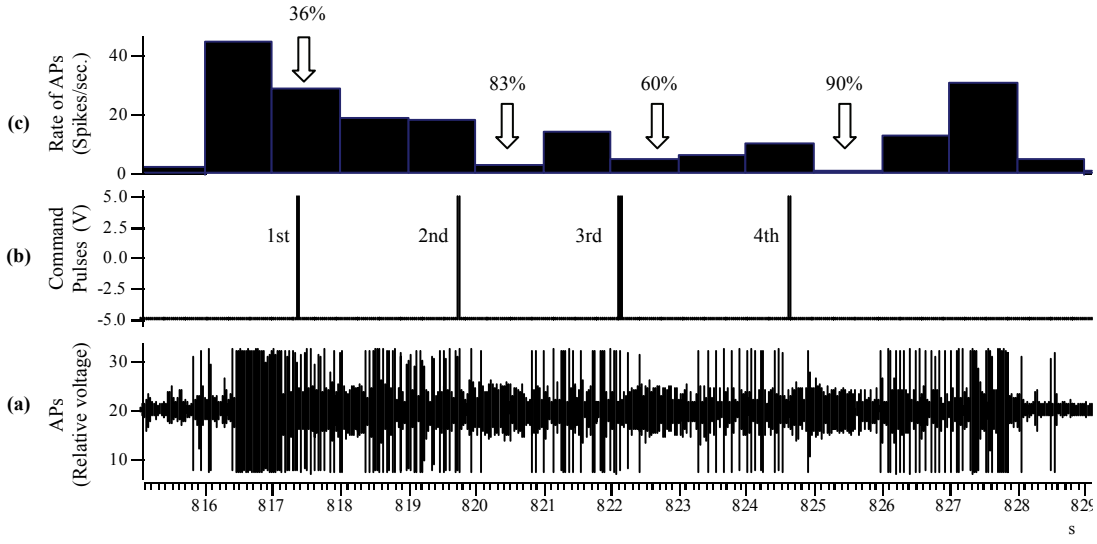

Figure 4.5 Inhibition effects with wireless ACC stimulation (Rat No. RT062707, cell No.2-2). (a) Rate of action potentials. (b) Command pulses of stimulation with 50 pulses, ±16V, 50Hz and 0.5-ms duration. (c) Recorded action potentials.

4.4 Stimulation with feedback loop

To demonstrate the feedback loop, several experiments were conducted using the Labview program described in Chapters 3.4. Before the feedback loop was applied, the APs, during pressure stimulus from a neuron, were recorded using Spike2. As shown in Fig. 4.6, the rate immediately rose above 100 spikes/sec. at the beginning and gradually decreased to around 50 spikes/sec. at the end of the stimulus.

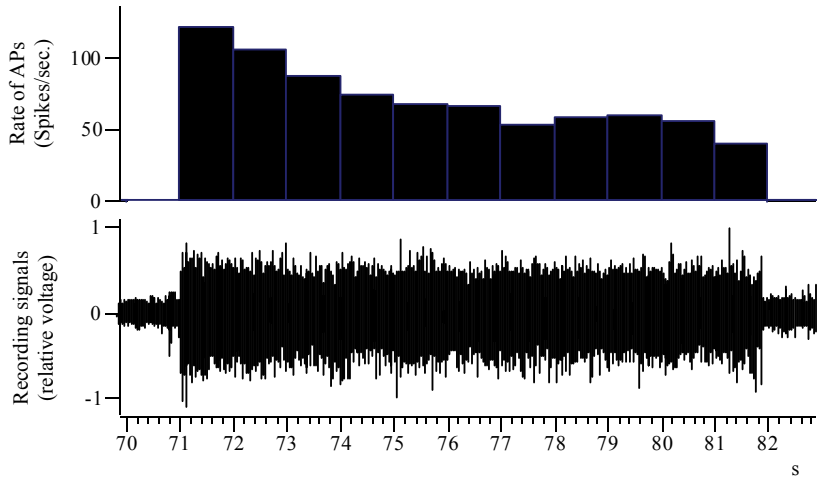

Figure 4.6 Rate of APs during pressure stimulus without a feedback loop (RAT No. RT100507-2).

To apply the feedback loop, a pain time slot and rate threshold needed to be set. In this first demonstration, the pain time slot was 3 seconds and the rate threshold was 150 spikes during the 3 seconds. Note that the rate threshold was set in the Labview program which is not necessary the same number as shown in the Spike2. The stimulation parameters were fixed at ±2.6V, 140 pulses, 0.7ms duration and 7ms interval at the PAG. Figure 4.7 shows the rate of APs from the same neuron after the

feedback loop was applied. From the results, the rate increased above the threshold and the 1st stimulation was activated. Although the rate of APs reduces 54%, during the stimulation, the total rate of APs in the 3 second time slot was still higher than the threshold, resulting in the 2nd stimulation. The 3rd and 4th stimulation was also activated with the same mechanism.

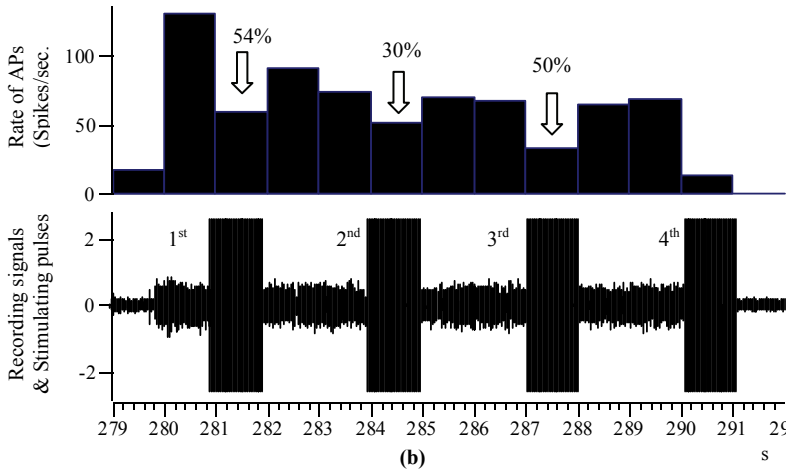

Figure 4.7 Rate of APs during pressure stimulus with fedback loop (RAT No. RT100507-2).

More recordings were performed for preliminary studies of the feedback loop mechanisms. The results of automatic stimulation with fixed stimulating pulses are shown in Fig. 4.8. The stimulating parameters were ±2.6V, 100 pulses, 1.0ms duration and 10ms interval applied to the PAG area. The closed-loop pain relief mechanism can be explained in 4 steps. In the 1st period, the mechanical stimulation was applied resulting in a high rate of APs representing severe pain. The high rate exceeded the pain

threshold. The the stimulation was activated in the 2nd period. In this period, the APs were inhibited by the stimulation and the rate of APs reduced resulting in the pain relief.

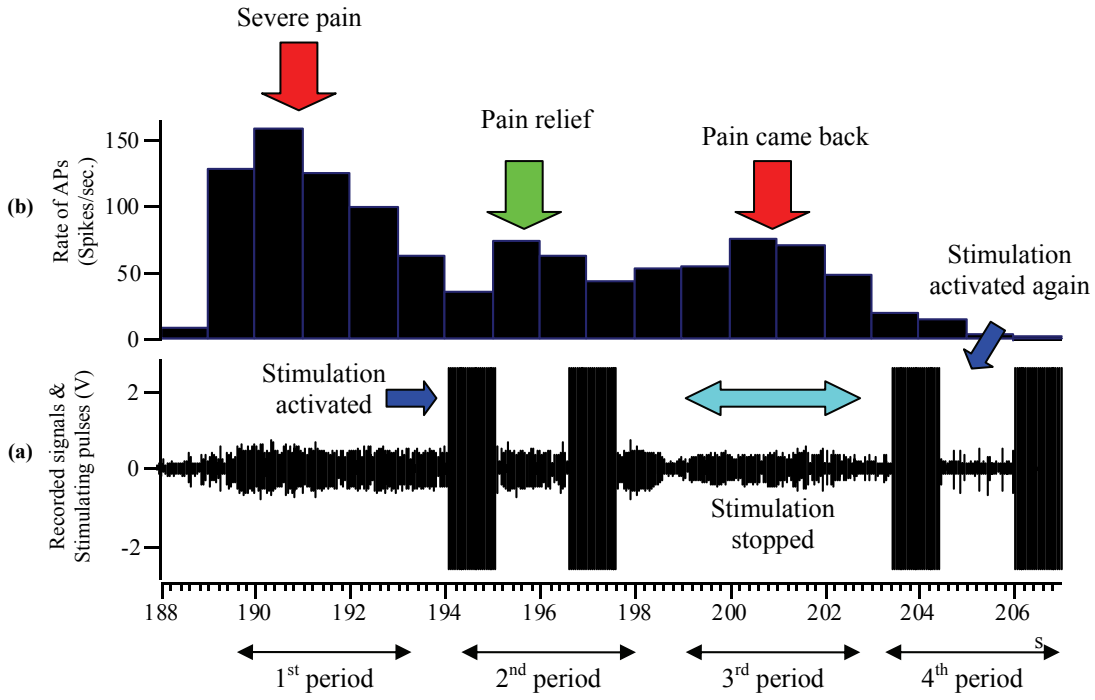

Figure 4.8 Automatic pain reduction using fixed stimulating pulses (Rat No. RT100507-3). (a) Recorded signal and stimulating pulses. (b) Rate of action potentials.

Another stimulating pulses train was activated until the rate was less than the threshold and thus the stimulation stopped in the 3rd period. When the stimulation stopped, the rate of APs increased which means the pain gradually came back. Once the rate was higher than the threshold, the stimulation was activated again as shown in the 4th period. The mechanism will be continued until the pain is completely vanished.

Another experiment shows the stimulation with multiple doses when the 1st trial is not effective. In this experiment, two set of stimulation parameters will be used for

PAG stimulation. The first set was ±1.3V, 100 pulses, 0.5ms duration and 10ms interval which was considered a light dose. The second set was a stronger dose with ±2.6V, 200 pulses, 1.0 ms duration and 5 ms interval. When the stimulation was activated, the light dose will be applied first, and if it was not effective, the strong dose will be used for the rest of the stimulation. The results are shown in Fig. 4.9.

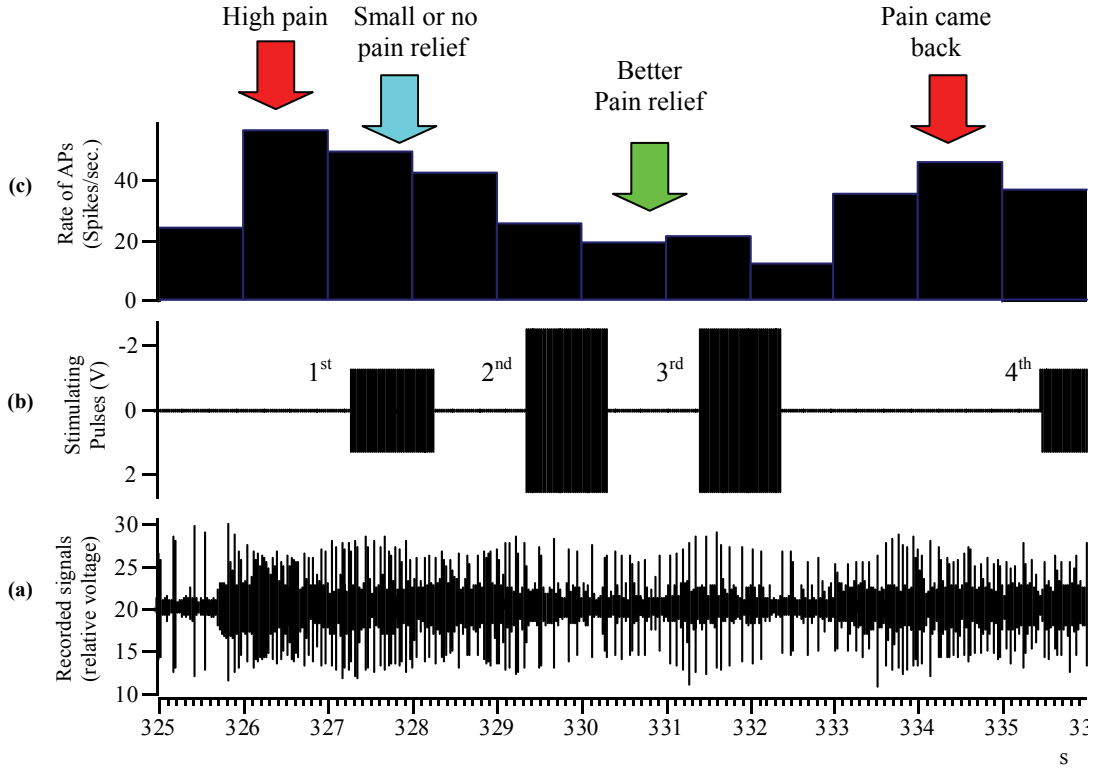

Figure 4.9 Automatic pain reduction using multiple stimulating doses (Rat No. RT101207-3). (a) Recorded signal. (b) Stimulating pulses. (c) Rate of action potentials.

When the high pain occurred (at the 326th s), the stimulation was activated with ±1.3V. However the stimulation did not decrease the pain level effectively. The rate of APs was still higher than the threshold. The 2nd and the 3rd stimulations with ±2.6V were thus activated. After the 3rd stimulation, the rate of APs decreased lower than the

threshold and the stimulation stopped. When the pain came back, the new cycle continued again with the 4th stimulation staring from ±1.3V stimulation.

4.5 Summary

In summary, a wireless pain management system was developed. The system can record and stimulate at the same time with features of feedback loop and decision making to activate the stimulation according to the recorded signals. The device is small enough to be carried by a rat. The device is capable of generating stimulating pulses with voltages up to ±18V. The preliminary results in anesthetized rats show the feasibility of using the device to study neuronal activities for pain management. From the experiments and results, there would be certain optimal stimulating parameters that give the highest inhibition. In general, more pulses, longer pulse durations, shorter pulses intervals and higher voltage levels give better inhibition effects. However, muscle contraction on the rats was observed when the stimulating doses were too high. This implies that the doses should be kept as low as possible in practice without sacrificing pain reduction. Given that the responses from different neurons and the differences between rats may vary, finding optimal parameters to inhibit pain at different potential brain areas then requires systematic experiments and statistical data to draw conclusion. Our next step is to conduct the experiment in freely moving animals. This wireless device can be used with various electrode configurations that are suitable for specific areas. This reported device provides a new tool for studying neuronal activities and potentially enables a new era of chronic pain relief in humans.

CHAPTER 5

INTRODUCTION TO A WIRELESS IMPEDANCE SENSOR FOR DETECTING GASTROESOPHAGEAL REFLUX

5.1 Motivation

Gastroesophageal Reflux Disease (GERD) is a medical condition that affects approximately 15% of the adult population in the United States and is one of the most prevalent clinical conditions afflicting the gastrointestinal tract. GERD refers to symptoms or tissue damage caused by the reflux of stomach acid into the esophagus and pharynx. The most common symptom of GERD is heartburn [5.1], but GERD can lead to complications such as esophageal cancer and lung damage. The two common forms of esophageal cancer are squamous cell carcinoma and adenocarcinoma. In the United States, esophageal carcinoma accounts for 10,000 to 11,000 deaths per year. Adenocarcinoma of the esophagus has the fastest growing incidence rate of all cancers.

Over the past 25 years, the incidence of esophageal cancer has increased 350%, faster than any other malignancy in the western world. One study showed that more difficult-to-treat esophageal adenocarcinoma cases are increasing 5% to 10% each year in developed countries [5.2]. The incidence of esophageal carcinoma is approximately 3-6 cases per 100,000 persons. These increased rates are strongly related to GERD which is the primary risk factor recognized [5.3]. Therefore, monitoring the GERD

symptoms comfortably and reliably becomes more important for early diagnosis of esophageal cancer.

5.2 Currently available and proposed methods for GERD diagnosis

Diagnosis of GERD can be simply empirical therapy such as life style modification. Endoscopy, manometry and ambulatory pH monitoring [5.4-5.6] need to be exploited in more complicated cases. Ambulatory of the esophagus helps to confirm gastroesophageal reflux in patients with persistent symptoms (both typical and atypical) without evidence of mucosal damage, especially when a trial of acid suppression has failed [5.7].

Recently, a combined monitoring of impedance/pH [5.8,5.9] and impedance/manometry [5.10,5.11] has been given more and more attention in clinical diagnosis. Esophageal impedance monitoring is a new technique used to detect episodes of gastroesophageal reflux that are both acidic and non-acidic in nature. This technique overcomes the limit of ambulatory pH-metry which does not always reliably detect the reflux of material whose pH value is more than 4.0. The bolus volume and position can also be determined by impedance monitoring [5.12,5.13].

Multichannel intraluminal impedance (MII) is a currently available instrument that has been used to correlate symptoms with episodes of gastroesophageal reflux. Whereas electric conductivity is directly related to the ionic concentration of the intraluminal content, materials with high ionic concentrations (e.g. gastric juice or food residues) have a relatively low impedance compared with that of the esophageal lining or air [5.13]. These can be measured by a differential AC voltage between each pair of

electrodes [5.14]. The electrodes used in the MII measurement are positioned on a catheter that is inserted transnasally into the patient's esophagus as shown in Fig. 5.1.

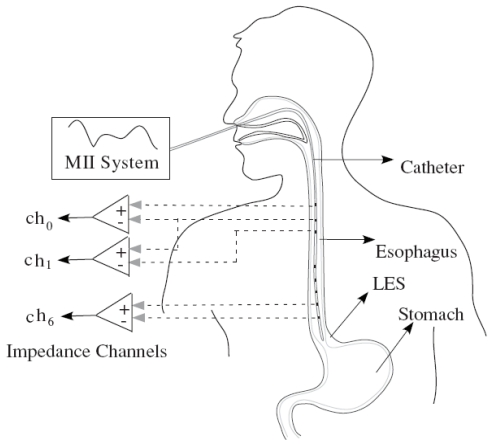

Figure 5.1 Multichannel intraluminal impedance catheter configurations [5.14].

A typical esophageal catheter is connected to an external electrical module for power and data acquisition through. Sensors are integrated along the catheter and the sensing membranes are exposed to air while the wires and/or chips are packaged in the tubing. Although the system brings more accurate monitoring results compared to the conventional ways, the configuration is bulky and uncomfortable for patients, features that may limit the clinical utility and accuracy of this technique for protracted monitoring of gastroesophageal reflux. A miniature wireless device that does not require tethered external connections is thus preferred for esophageal reflux monitoring. To date, a wireless pH monitoring device has been developed [5.15]. The systems utilize RF transmitter and do require a battery. Although the wireless module eliminates

tethered connections and makes patients feel more comfortable, the monitoring time is limited by the battery and only applies pH value variations.

In this work, a passive telemetry has been proposed to achieve wireless impedance sensing. The final goal is to develop a small passive sensor, without the need of integrating a battery, on a flexible substrate that attaches to the esophagus walls. The system consists of an implanted device and an external reader as shown in Fig. 5.2. Two approaches were proposed to realize passive sensing of the acid reflux. The first method relies on the resonance frequency shifting of passive components on the implant which can be measured by amplitude detection. The second approach utilizes RFID principles to detect the frequency generated from a circuitry on the implant powered by an external reader.

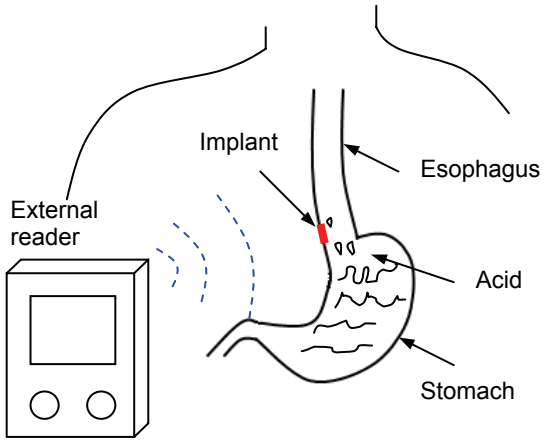

Figure 5.2 Schematics of an implant and an external reader for wireless impedance sensor.

CHAPTER 6

AN IMPEDANCE SENSOR USING AMPLITUDE DETECTION

6.1 Operation principles

A method to measure impedance changes using passive telemetry is proposed. The approach is based on inductive links between two coils - an external coil connected to an RF (radio frequency) source forming a resonant circuit and a small implantable coil connected to an interdigitated electrode impedance sensor. The resonance changes as the mutual inductances change, reflecting the impedance changes in the esophagus caused by fluid passing the electrodes. Measurement of the resonance frequency commonly has been used to detect the change of mutual inductance [6.1,6.2]. However, this requires frequency scanning that involves complex and expensive electronics. a simpler and less costly way is proposed to detect impedance changes in the implanted coil by using differential amplifier circuits as shown in Fig. 6.1.

The external coil and the implanted coil have the inductances of L_1 and L_2, respectively. The external coil is connected to a capacitor C_1 in series to form a resonant circuit which induces a high voltage on the external coil to deliver the power to the implanted coil. The implanted coil is connected to the electrode to measure the impedance of the esophagus. The equivalent circuit of the interdigitated electrode, when placed in the esophagus, is simplified to a resistor, R_3, and a capacitor, C_3, in parallel.

Accurate modeling of living tissues can be found using the parameters in [6.3]. In this work, a simpler model to demonstrate the principle was used. A capacitor, C_2, is also used to make a resonany circuit at the implanted coil to reflect the energy back to the external coil.

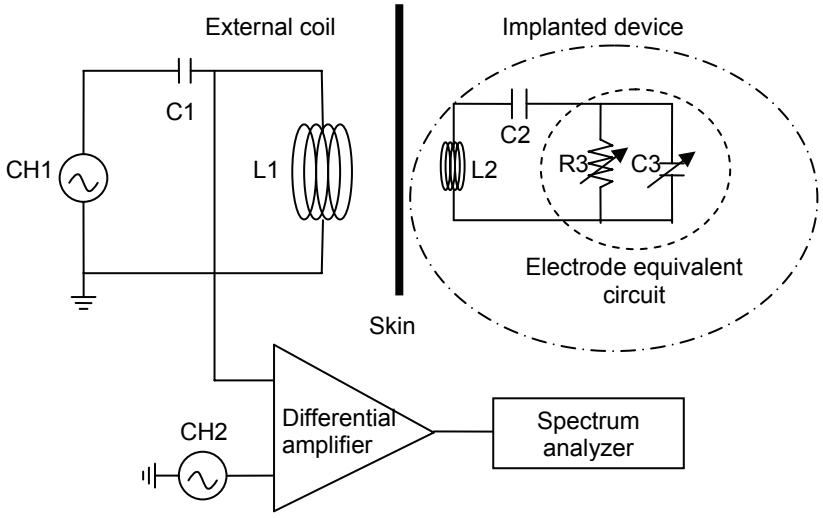

Figure 6.1 Simplified circuit diagram to detect impedance changes at the implant.

The circuits are first tuned by setting the frequency of the voltage source CH1 to the resonant frequency of L_1 and C_1. The high voltage at the external coil is tapped into the differential amplifier circuits by a voltage divider to reduce the signal level to the operational range of the amplifier. The voltage source CH2 with the same frequency is tuned to the same phase and amplitude of CH1 voltage at the differential amplifier input. The output of the differential amplifier is therefore close to zero. Tuning is done when there is nothing on the implanted coil as a baseline measurement. Once reflux occurs, the electrode impedance (R_3,C_3) will be changed. The mutual inductance

between both coils is disturbed and the differential amplifier circuits are out of tune, resulting in higher amplitude at the spectrum analyzer. The output amplitude is thus directly related to the impedance of the refluxate on the electrode, and therefore, wireless impedance sensor functionality is achieved.

6.2 Implanted coil design

The implanted coil was fabricated on a flexible Kapton substrate to attach onto the esophagus wall. The implanted method presented in [6.4] can also be used for this device. The implant device includes both coil and sensing electrodes with an equivalent circuit shown in Fig. 6.1. The physical structure of the planar device is shown in Fig. 6.2(a). The planar coil is placed in the outer area to maximize the inductance, and the electrodes are placed at the center. The electrodes are chosen to be interdigitated fingers which increase contact areas achieving high sensitivity. A fixed capacitor (C_2) is placed in series with the coil (L_2) and the electrodes (R_3,C_3). The capacitance of C_2 is calculated from the resonant frequency generating at the external coil using the equation:

$$f_{external\,coil} = \frac{1}{2\pi\sqrt{L_2 C_2}} \tag{6.1}$$

When the electrode is exposed to air, the resistance *R3* is very high (as an open circuit) and the capacitance C_3 is much lower than C_2. The total capacitance seen by the coil is thus close to the capacitance of the air surrounding the electrodes (Fig. 6.2(b)). The resonant frequency at this state is far from that of the external coil, and thus the implant has no effect on the external coil. This is the baseline condition used for tuning

the amplifier circuits. When the electrodes are exposed to acidic solutions, R_3 decreases (toward a short-circuit condition), and C_3 is much higher than C_2. The total capacitance is thus equal to C_2 (Fig. 6.2(c)). During this condition, the resonant frequency of the implant is equal to that of the external coil (from the Eq. 6.1). The mutual inductance of this state is the highest, and thus the differential amplifier is detuned, resulting in the maximum output amplitude at the receiver. Output amplitudes between these two conditions indicate impedance values between air and acid.

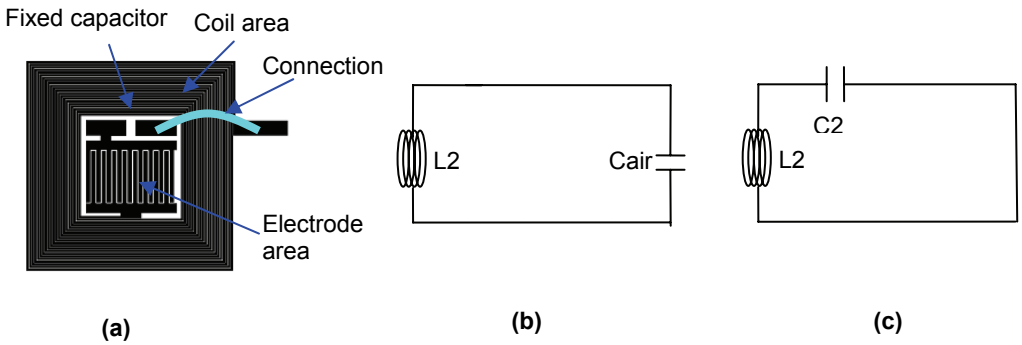

Figure 6.2 (a) Layout of the implanted coil. (b) The equivalent circuit in air. (c) The equivalent circuit in acid.

6.2.1 Electrode measurements

There are 4 clinical categories of reflux measured by a conventional impedance catheter: (1) acid reflux, (2) superimposed acid reflux, (3) weakly acid reflux and (4) non-acid reflux [6.5]. In this work, the focus is on the ability to distinguish between acid and non-acid reflux. Three electrodes were fabricated to investigate the performance of the interdigitated structures. Each design has the total area of 1×1 cm^2 with different finger widths and spacings. The capacitances of the electrodes when immersed in air,

city water and simulated stomach acid (70:1 and 50:1 muriatic acid) were measured and are shown in Table 6.1.

Table 6.1 Capacitances of each electrode design in different solutions.

Conductor width/spacing	1000 μm/100 μm	500 μm/50 μm	250 μm/50 μm
Air	2.7pF	5.3pF	9pF
City water	43pF	77pF	116pF
Stomach acid (70:1)	> 1μF	> 1μF	> 1μF
Stomach acid (50:1)	> 1μF	> 1μF	> 1μF

Note that the capacitance of the electrodes in air is much lower than that in water and acid. The capacitance in acid reaches the μF ranges for all designs, which is much higher than those in air or water. This agrees with our hypothesis. The results show that smaller finger spacing and narrower finger width (which means more fingers) result in higher capacitance for electrodes with the same total area. The dimensions of the electrodes can be carefully adjusted to achieve a desired sensitivity for specific impedance measurements.

6.3 External coil

For ranges of a few centimeters, the high attenuation of RF signals in biological tissues mandates carrier frequencies below 10MHz [6.6]. The resonance frequency around 1MHz was chosen to avoid high RF attenuation. As shown in Fig. 6.3, the external coil was fabricated on a PCB board using conventional photolithography

techniques. Rogers RO3003 with a dielectric constant of 3.0 and a copper thickness of 35μm was used. The PCB thickness was 1.52mm. The planar rectangular coil has 20 turns with a 300-μm width and a 200-μm spacing. The outer perimeters were 6 cm × 6 cm. The inductance calculation of a planar coil has been demonstrated in [6.7,6.8]. The calculated inductance was 38μH while the measured inductance was 47.32μH. The discrepancy may be due to the undercut etch of the thick copper foil of the PCB, which can easily reduce the conductor width by 70μm. A capacitance of 330pF was chosen and connected to the coil in series. The measured resonant frequency was 1.02MHz with a quality factor (Q) of around 7.

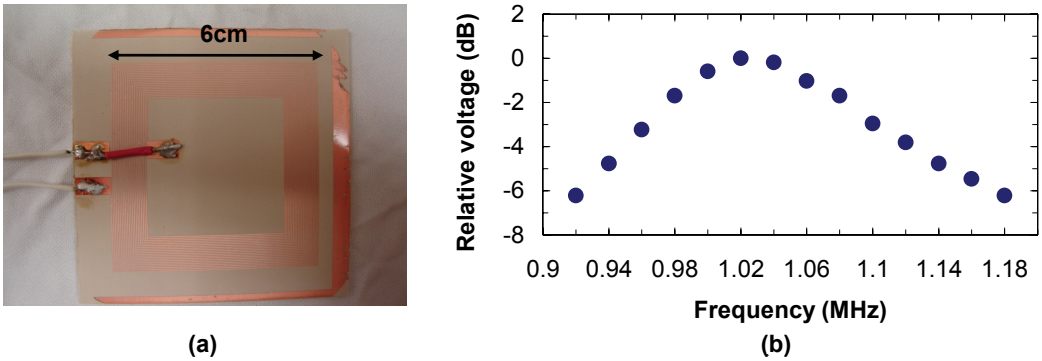

Figure 6.3 (a) External coil. (b) The measured frequency responses.

6.4 Fabrication of the implanted coil

The fabricated coil has a dimension of 2×2 cm^2. The coil has 20 turns with a conductor width of 200μm and a 50-μm spacing between lines in each turn. The electrodes consist of 17 interdigitated fingers which are 0.4mm wide and 5mm long, with a 0.1-mm spacing. The coil and the electrodes were fabricated together by standard

photolithography processes [6.9-6.11] as shown in Fig. 6.4. First, a 2000-Å seed layer of Cu was thermally evaporated onto a Kapton substrate (Fig. 6.4(a)). Photoresist NR7-3000P was spin coated, baked and patterned for the coil and the electrodes mold (Fig. 6.4(b)). A seed layer of Cr/Cu/Cr or Ti/Cu/Ti can be used for better adhesion of Kapton/Cu and Cu/photoresist interfaces. The thick photoresist layer was achieved by two layers of NR7-3000P with a spinning speed of 1000 rpm for 30 seconds. The baking temperatures and times of the 1st and 2nd layers are 120˚C/1min and 150˚C/ 1min 20sec, respectively. Then the sample was exposed to UV light and baked at 120˚C for 70sec. The baking was done in an oven to evenly heat up the photoresist on the non-flat substrate.

The sample was put in a Cu electroplating solution for 2 hours with an electrical current of 10 mA. A Cu layer of about 8 μm was formed (Fig. 6.4(c)) to achieve low resistance. The photoresist was removed by putting the sample in an ultrasonic bath with acetone for 10 min and then the Cu seed layer was etched away (Fig. 6.4(d)). A 10-μm thick layer of SU-8 was spun, patterned and then hard cured onto the coil area to prevent undesired electrical contact (Fig. 6.4(e)). A jumper wire was used to complete the circuit of the coil and the electrodes. This also can be done by depositing a metal airbridge with first thermal evaporator and then electroplating processes. The sample was then Ni electroplated to protect the Cu electrode from corrosion in acid (Fig. 6.4(f)). The coil inductance was measured as 9.41μH, which is close to the theoretical value of 9.1μH [6.8]. The measured DC resistance of the coil is 13Ω resulting in a calculated quality factor (Q) of 4.63 using the equation $Q = \omega L/R$, where ω is the

angular frequency. The Q value can be improved by plating a thicker Cu layer to reduce the coil resistance. The capacitance for the resonant frequency at 1.02MHz was calculated to be 2587pF. An SMD (surface mount device) capacitor of 2200pF, the closest value available, was selected and soldered onto the sample. A metal-insulator-metal (MIM) capacitor can be fabricated instead to achieve the exact capacitance in the future without using the hybrid components. The final device is shown in Fig. 6.4(g).

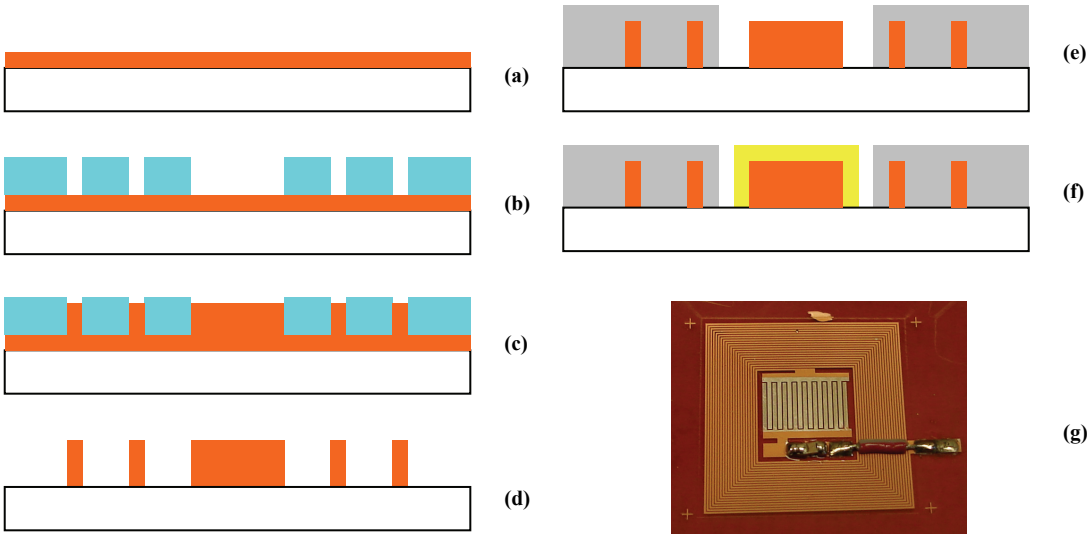

Figure 6.4 (a)-(f) Fabrication processes for the implanted coil. (g) A photo of the fabricated coil on a flexible substrate.

6.5 Experiments

6.5.1 Wireless impedance sensing

The experiment was done by putting the implant in a 3-cm diameter glass tube to simulate conditions in the esophagus. The implant was suspended in the center of the tube using a plastic sheet as shown in Fig. 6.5(a). In clinical applications, the implant

devices will be attached to the esophagus using clips [6.4]. The external coil was placed outside of the tube at a distance of 3cm from the implant. The external coil was connected to an amplifier in a shield box as show in Fig. 6.5(b). The test solutions were supplied through another tube. The input signal at CH1 was at 1.02MHz sine wave with an amplitude of 3Vp-p, resulting in about 12Vp-p at the external coil. The voltage source CH2 was adjusted at the same frequency with an amplitude of 2.114Vp-p and +146.34˚ phase shift.

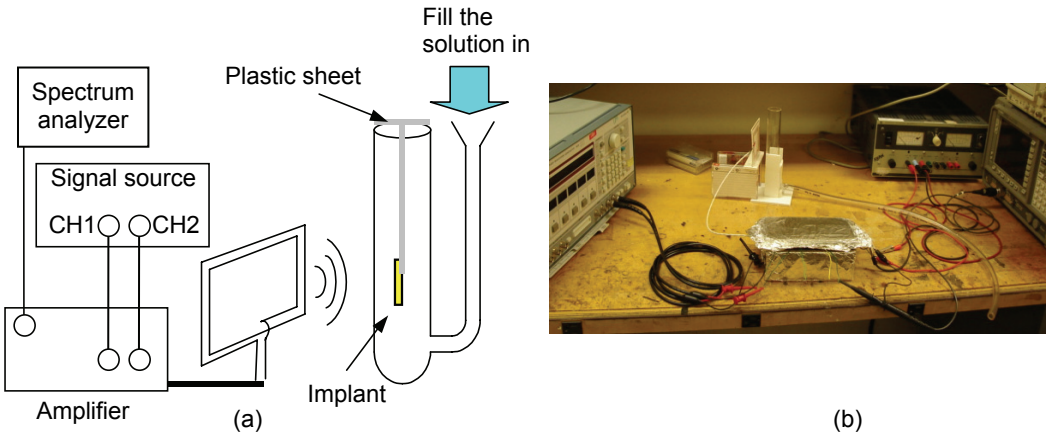

Figure 6.5 (a) Schematic experiment set up. (b) A photo of the equipment setup.

The differential amplifier with a total gain of 370 gave an output of around 11mV as the baseline condition. The outputs from the spectrum analyzer when air, water and simulated stomach acid were on the electrodes were 11mV, 15mV and 29mV, respectively, as shown in Fig. 6.6(a-c). Simulated stomach acid of 70:1 and 50:1 muriatic acid gave the same results. The output amplitude can be increased by adding more amplifier stages in the circuit. These output values represent the impedances of

non-acid and acid reflux where the reflux with an impedance between water and acid will fall in the range of 15-29 mV. The output amplitudes were plotted again in Fig. 6.6(d) to compare the reading in different conditions of the reflux.

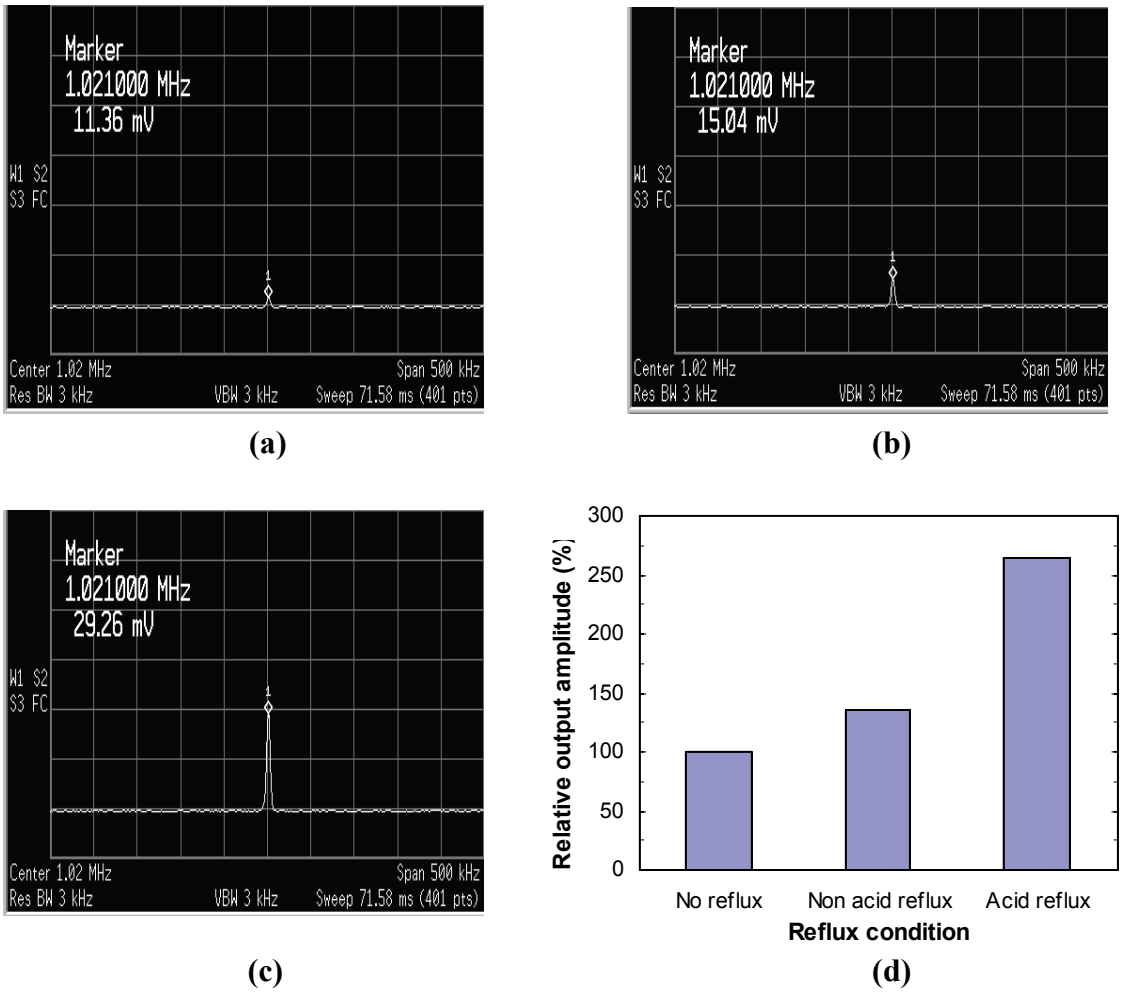

Figure 6.6. Output spectrum for (a) air, (b) water, (c) simulated stomach acid and (d) relative plot.

When exposed to acid, an output of more than 50mV was observed immediately after the acid solution was removed. This phenomenon shows that the wireless signal drops when acidic solution is present between the external coil and the implant. This

attenuation was not observed in the case of water, which has much less ionic content and hence much lower conductivity than the acidic solution.

6.5.2 Attenuation in human tissue

The propagation effects by a layer imitating tissues between the implant and the external coil were studied. The operating frequency was lowered to 850kHz by increasing the value of resonant capacitors on the implant and the external coil. A lower carrier frequency helps reduce the attenuation of RF signal in human tissue. The implant was laid down and the external coil was set up horizontally above the implant. The distance of the external coil was kept at 3cm from the implant. A 1-cm layer of liquid was applied onto a plastic tray sitting 2mm above the implant. It was observed that neither water nor acid as the liquid layer had noticeable effects on the received signal amplitudes. This is to imitate the wet tissue effect on the RF signal propagation. Another experiment was done by flooding the implant with acid directly by putting it into the tray and the attenuation of the signal could be quantified. The signal dropped to 80% when 2mm thick acidic fluid was flooded onto the implant. More acid was poured onto the implant and the signal reduced to 78% when the acidic fluid layer was 1cm thick. The results are compared in Fig. 6.7.

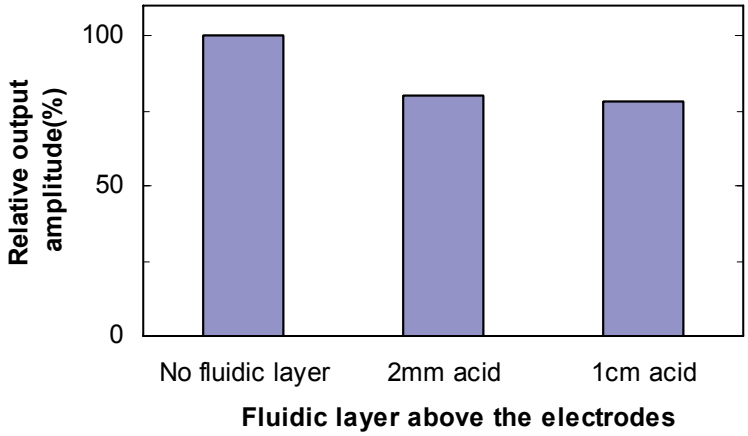

Figure 6.7 Effects of conductive fluid above the implant.

These results show that the inductive link at 850kHz was slightly affected by a conductive fluid layer imitating wet tissues. This is due to the fact that the magnetic field is capable of penetrating a non-magnetic conductor. Small distortion of signal waveforms due to the spectral characteristics of tissues is expected. However, the distortion will not be significant in determining the relative impedance changes.

6.6 Summary

In this chapter, we describe a wireless sensor that we propose to implant in the esophagus of patients to detect impedance changes associated with gastroesophageal reflux. Our preliminary results are promising, and the device appears to be capable of distinguishing the reflux of nonacidic and acidic materials. Signal amplitudes increased by 36% and 163% from baseline when the device was exposed to nonacidic and acidic solutions, respectively. The sensitivity of the sensor to detect reflux can be adjusted by changing the electrode design. The size of the implant can be reduced and its

performance can be improved by using thicker coils to decrease the coil resistance and using the exact value of the capacitors for better resonance frequency tuning. Multilayer coil and magnetic materials also can be used for future investigation.

CHAPTER 7

AN IMPEDANCE SENSOR USING FREQUENCY DETECTION

7.1 Operation principles

The approach in chapter 6 is, in fact, subjected to major problems in practical uses. The devices that rely on mutual inductance are susceptible to noise, and the relative accuracy will vary with the distance between the coils due to different body types and the body movement of the patient. For this reason, a new impedance sensor platform was proposed. It adapts radio frequency identification (RFID) technology including a transponder and a reader. A commonly used modulation technique in RFID, frequency shift keying (FSK), is applied. The FSK allows for a simple reader design and provides very high noise immunity [7.1]. It is less susceptible to the misalignment in coupling coils and artifacts from motion, which are two major problems in biomedical implants [7.2].

As in proximity RFID [7.3], our system is based on inductive coupling between two coils. In Fig. 7.1(a), the reader coil generates electromagnetic fields coupling into the transponder coil. Both coils are connected to a capacitors forming resonance at the same frequency. In the near field region, the impedance seen by the reader coil changes, when the switch at the transponder opens or closes. This load modulation alters the voltage level at the reader coil. The frequency source at the reader is adjusted to the

resonance frequency resulting in high amplitude signals at the reader coil. This frequency is usually much higher than that of the switching frequency at the transponder.

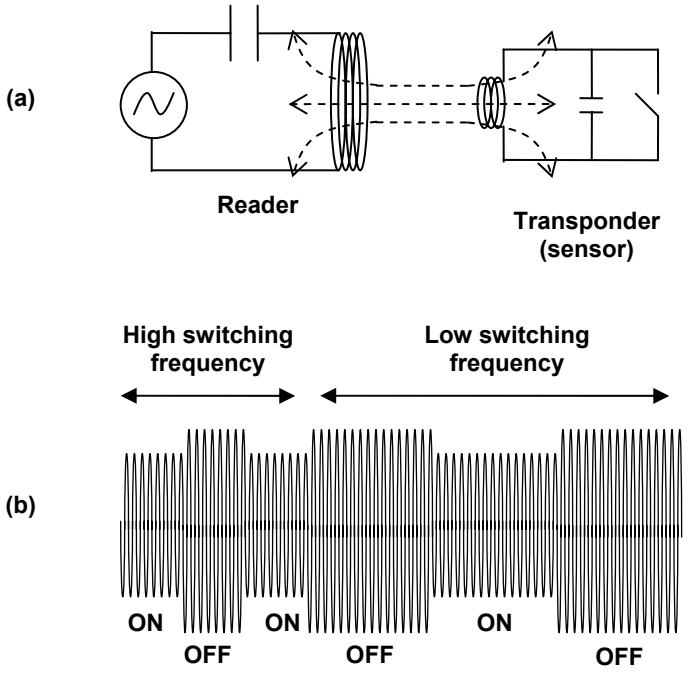

Figure 7.1 (a) Schematic diagram of the systems operation principles.
(b) Signals at the reader coil.

Figure 7.1(b) shows the signals at the reader coil. When the switch at the transponder is open (OFF), the signal amplitude at the reader keeps high amplitude due to low loading effects. When the switch is close (ON), the transponder loads the reader coil and the reader is shifted from resonance condition. Thus the signal amplitude reduces. The switching frequency at the transponder varies with sensor conditions. When the impedance of the sensor is high the switch turns on and off with low frequency and, when the impedance of the sensor is low the switch turns on and off

with high frequency.As a result, the transponder switching frequency can be extracted at the reader using envelope detection. In this case, the switching frequency is controlled by the electrode impedance, and therefore, a wireless batteryless impedance sensor is achieved.

7.2 Transponder architecture

Fig. 7.2 shows the transponder block diagram. The front end is an antenna and a capacitor forming a resonant circuit to receive powers and modulate the data. The voltage multiplier and the regulator build up a constant DC level to operate the rest of the circuit. The frequency generator transduces the impedance to frequency-varying signals. By connecting the electrodes to the frequency generator, the output frequency can be controlled by the impedance of the materials on the electrodes. This signal turns the switch on and off. With this technique, the data from the sensor can be reconstructed from the frequency detected at the reader.

With current advances in IC technologies, all circuitry with the resonant capacitor can be integrated into a single chip with the size of few millimeters. The transponder could be finalized in several platforms which includes a small chip, an antenna, and an electrode. The device can be packaged in a capsule or attached on a planar substrate with the coil antennas that are required to face the external reader in the appropriate direction as shown in Fig. 7.3.

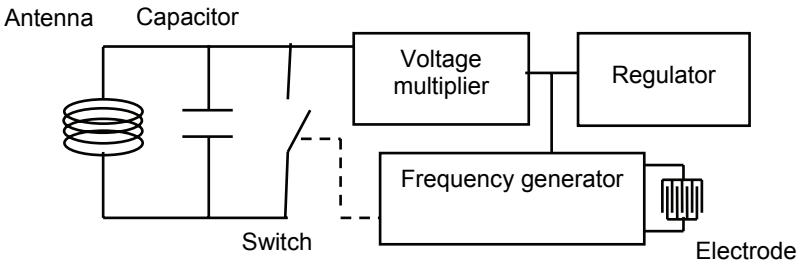

Figure 7.2 Block diagram of the platform.

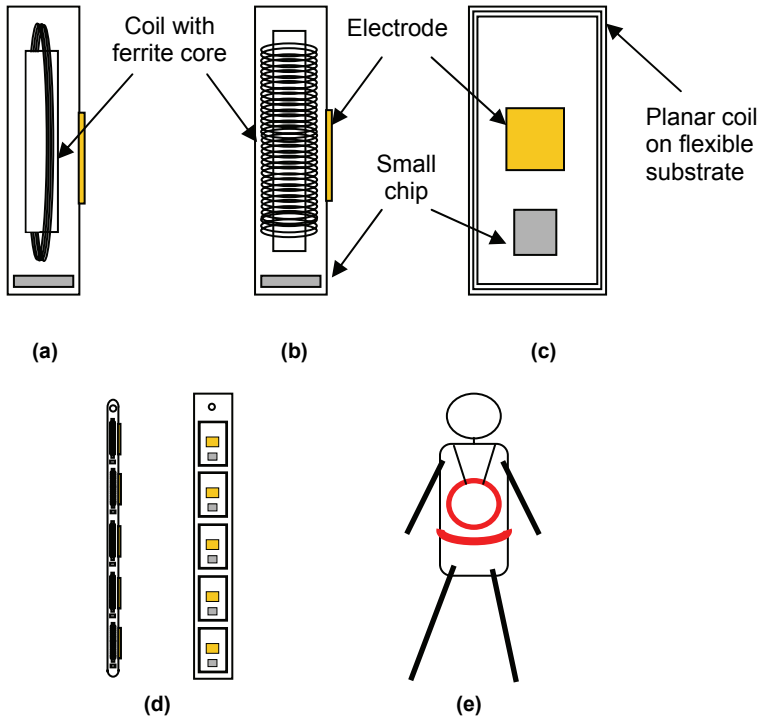

Figure 7.3 Possible platforms of wireless batteryless impedance sensor. (a) Capsule with vertical antenna winding. (b) Capsule with horizontal antenna winding. (c) Planar platform. (d) Sensors array in a flexible tube or strip. (e) Possible necklace or belt for an external reader.

Figure. 7.3(a) shows a capsule platform with a ferrite core antenna winding vertically inside the capsule frame to receive maximum energy from the reader. The

horizontal winding in Fig.7.3(b) reduces the energy coupling efficiency because of the small cross section area; however, this makes the device more orientation independent. Fig. 7.3(c) shows the planar platform where the antenna is fabricated on a thin flexible substrate and the chip and the electrode in the middle. Multiple sensors can be packaged in a flexible tube of strip as shown in Fig. 7.3(d). The external reader could be made in a form of a necklace or a belt as shown in Fig. 7.3(e).

Due to the high development cost of a small chip, the working mechanism of the transponder will be demonstrated using discrete components on a printed circuit board (PCB). A prototype was assembled on a PCB. 4-layer PCB was chosen to get a compact platform and less EMI problems as shown in Fig. 7.4. In this thesis, it will be referred as Gen-1 impedance sensor.

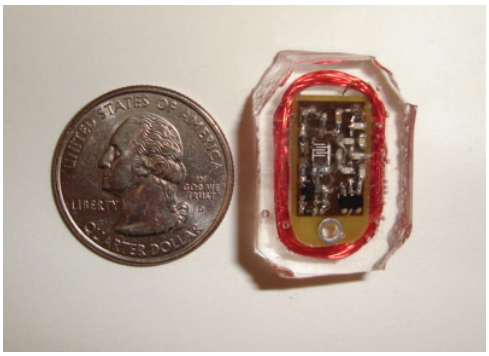

Figure 7.4 The Gen-1 wireless impedance sensor prototype.

The interdigited electrode was designed using PCB traces. The overall size can be very small using SMD components. An inductor of 15μH was made from a 30AWG magnet wire winding around the PCB to realize the antenna. When connected to a

capacitor of 1000pF, the calculated operating frequency is 1.3MHz. It was then coated with Polydimethylsiloxane (PDMS) to prevent a short circuit on the circuitry that could be caused by reflux. A small window was cut open for the electrode to make a contact to the reflux for impedance sensing.

7.2.1 Voltage multiplier and Regulator

For inductive coupling over a distance r, the voltage induced across the transponder antenna reduces by $1/r^3$ [7.4]. The received voltage usually becomes too low to operate the circuitry on the transponder. A series of diodes and capacitors have been thus deployed to form a voltage multiplier [7.5]. This technique is commonly used in UHF RFIDs and helps increase the read ranges dramatically. The voltage multiplier, however, has a low power conversion efficiency which varies with load currents [7.6]. Therefore, the number of multiplier stages is limited.

In this work, general purpose diodes MMBD4448 and 100-pF capacitors were chosen in a 4-stage voltage multiplier as shown in Fig. 7.5. A matching network was not needed because of the low operating frequency. The capacitance value and the number of stages were roughly estimated from OrCAD PSpice and optimized experimentally to achieve the longest read range. The output of the voltage multiplier was connected to a Seiko Instruments (S-812C25AY-B-G) 2.5-V CMOS regulator which consumed less than 2μA current. A 12-V zener diode is added to protect the regulator from high voltages in case the transponder is very close to the reader. A 1-μF storage capacitor was placed at the regulator output to keep the voltage stable during modulation.

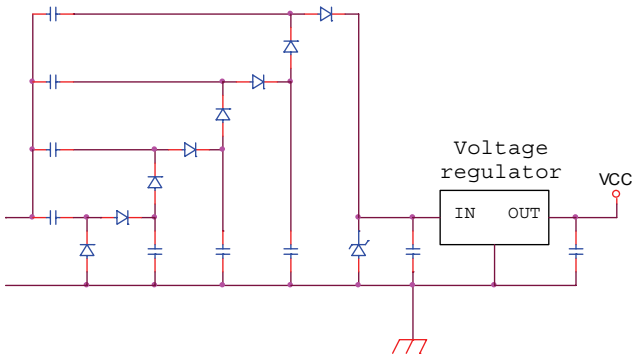

Figure 7.5 Voltage multiplier and regulator.

7.2.2 Frequency generator and Modulator

A relaxation oscillator circuitry was selected, which consists of a comparator, a capacitor and few resistors. This oscillator generates an output frequency based on the RC time constant in the circuit [7.7]. Fig. 7.6 shows the circuit topology in which the electrode is represented by a variable resistor R_S and a variable capacitor C_S in parallel.

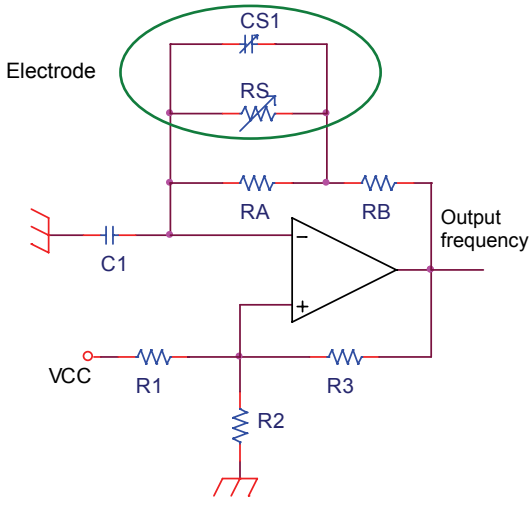

Figure 7.6 Relaxation oscillator.

The resistors R_A, R_B and the capacitor C_1 keep the output frequency in the desired range. A low-power op-amp LPV321 (Texas Instrument) was used as a comparator. The resistors R_1, R_2, R_3, R_A and R_B were 10MΩ, 1MΩ, 750kΩ, 12.4kΩ and 10kΩ respectively. The capacitor C_1 was 1nF.

To modulate the data back to the reader, the frequency generator was connected to the gate of a MOSFET M_1, as shown in Fig. 7.7 where Vcc is the regulator output voltage. L_1 and C_1 are the transponder antenna and the resonance capacitor respectively. It is important that the modulation must begin after Vcc reaches the regulated voltage. This will keep the frequency generator outputs stable. Moreover, when the modulation occurs, the storage capacitor discharges. Therefore, more energy is required in order to build up the voltage, and the read range will be reduced dramatically.

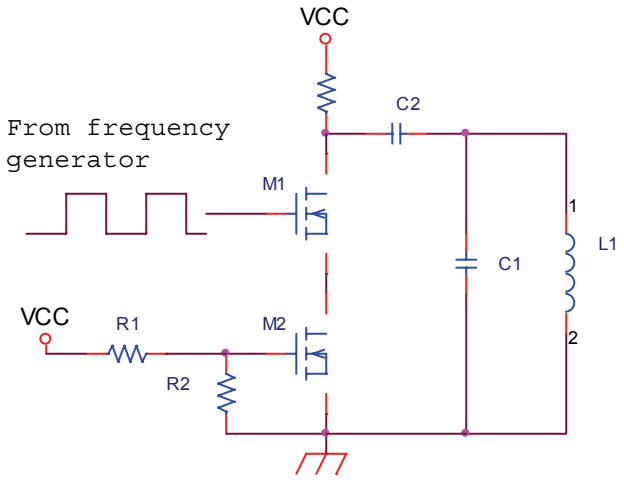

Figure 7.7 Modulation circuit.

To prevent these problems the transistor M_2 was placed at the source of M_1. It will turn on only when Vcc reaches the regulated value. The resistors R_1 and R_2 were added to form a voltage divider to step down the Vcc level to the threshold voltage of M_2. When M_2 is turned on, M_1 behaves as a switch turning on and off by the signals from the frequency generator. When M_1 is off, L_1 and C_1 resonate at the same frequency as that of the reader. When M_1 is on, the capacitor C_2 is connected to C_1 in parallel changing the resonance frequency. This variation causes the fluctuation at the reader coil and thus the modulation is achieved.

7.3 Reader

The analog front end of a general purpose RFID reader [7.8, 7.9] was modified to read the frequency-varying signal. The reader antenna was made from magnet wire wound around a foam bard. The reader circuit includes a power amplifier, which generates high electromagnetic fields coupling into the sensor, and an envelope detector to read the load modulation signals as shown in Fig. 7.8.

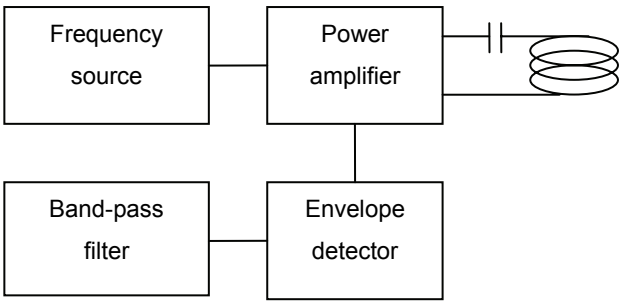

Figure 7.8 Rader block diagram and the coil signal.

The frequency source provides the carrier signal feeding the amplifier. The source is adjusted to the resonant frequency of the LC circuit resulting in a high voltage at the reader coil. When the modulation occurs, the voltage level at the reader coil fluctuates. The signal is extracted by the envelope detector and fed through the band-pass filter to extract the signal and suppress the high frequency carrier. After that the signal is amplified and processed easily. The output signal can be read from an oscilloscope or a spectrum analyzer.

7.3.1 Class-E power amplifier

In this work a class E power amplifier was chosen due to its high efficiency. The class E power amplifier has been considered in transcutaneous power transfer for many previous works [7.10-7.12]. The circuit diagram of a class-E amplifier is shown in Fig. 7.9.

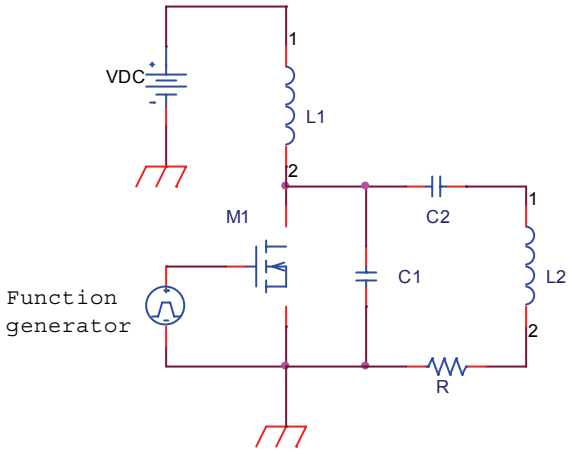

Figure 7.9 A class-E power amplifier.

The function generator provides 0-5V square wave signal to drive the MOSFET switch M_1. IRL510A was chosen due to its low threshold voltage. The dutycycle of 30% was chosen to minimize DC power consumption which will eventually be provided by battries. The design was based on 1.34MHz operating frequency where the recommended maximum permissible exposure (MPE) of magnetic field is the highest in the frequency ranges from 1.34MHz to 30MHz [7.13]. The operating frequecny could be changed according to the safety issues, performance and the allowed frequency band.

A coil antena with the size of 12×15cm was made from an AWG26 magnet wire winding around a foam board resulting in the inductance of 17μH with a Q of 70. Following the calculation procedures for the high Q appriximation in [7.14] the value of C_1 and C_2 were chosen to be 10nF and 900pF respectively.

7.3.2 Envelope detector

The envelope detector includes a diode and RC networks as shown in Fig. 7.10. The diode 1N4936 was chosen to retify the high voltage at the coil antenna of the class-E amplifier. The 100kΩ resistor and the 100pF capaitor has the time constant of 0.1MHz which is suitable for the carrier frequency above 1MHz. The 4.7 kΩ resistor and the 1nF capacitor form a low pass filter to reduce the DC signal level. The 1nF capacitor and the 100k resistor filtered high frequency carrier before the signal was fed to an op-amp buffer.

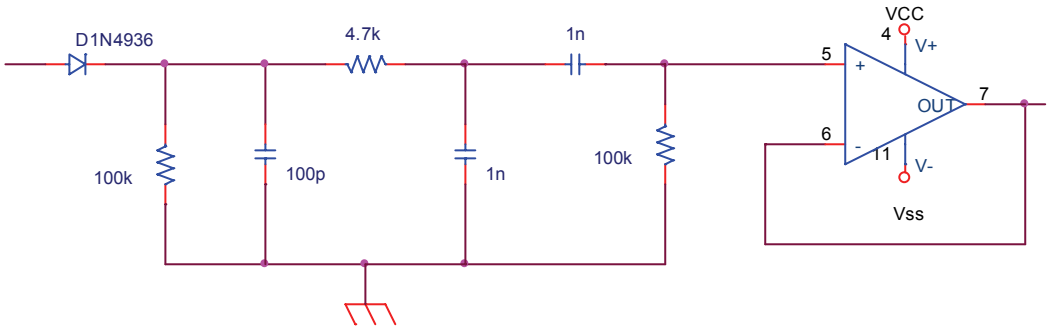

Figure 7.10 Envelope detector circuitry.

7.3.3 Bandpass filter

A unity gain butterworth bandpass filter was made. The circuit diagram is shown in Fig. 7.11. The calculated passband was around 500Hz to 75kHz which is wide enough for general purposes. After the band pass filter, the signal can be amplified and processed easily. Several amplifer stages using op-amps were used. Additional low pass filters were included in the reader to reduce the high frequency carrier that may couple into the circutry. At the final stage, a comparator was used to convert the sinusoidal signals to squarewaves which can be digitally processed.

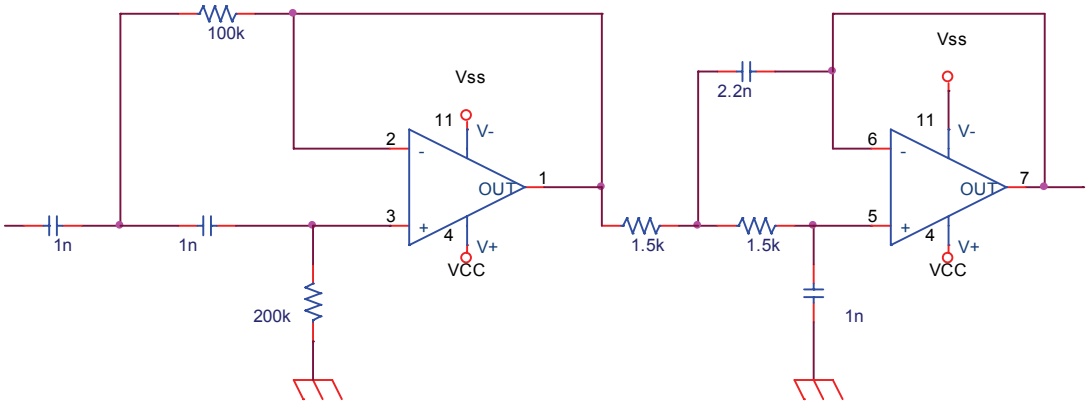

Figure 7.11 Bandpass filter circuitry.

7.4 Read range

The optimization of the read range for inductive coupling RFID was discussed in [7.15]. The transponder must receive enough power from the reader in order to operate properly. The reader, on the other hand, must have enough sensitivity to extract the signal from the transponder. The read range thus depends on the noise level in the environment as well. In general, using a higher current and larger antenna at the reader, or making lower power sensor circuitry, or enlarging the transponder antenna will satisfy the power requirement at a longer distance. Making a high Q transponder antenna improves the power coupling efficiency but suffers from frequency shifts caused from manufacturing tolerance of other components. In a similar manner, although high Q reader antenna improves the reader sensitivity, it is also subjected to noise in the environment increasing the possibility of a wrong reading. The typical read ranges of inductive coupling RFID devices are shown in Fig. 7.12 [7.8,7.9].

Another consideration for the read range is the duty cycle of the modulation signals from the transponder. As explained in the Chapter 7.2.2, when the switch turns on to modulate the data, the transponder cannot receive the power from the reader and the circuit must operate from the charges remaining in the capacitor. For this reason, one can reduce the duty cycle of the modulation (reduce the switch turn on time) to conserve more power from the reader; however, the reader must have very high sensitivity to read the weak modulated signal. Considering the available power from the reader, the reader sensitivity and the power consumption of the transponder, the optimum results can be obtained.

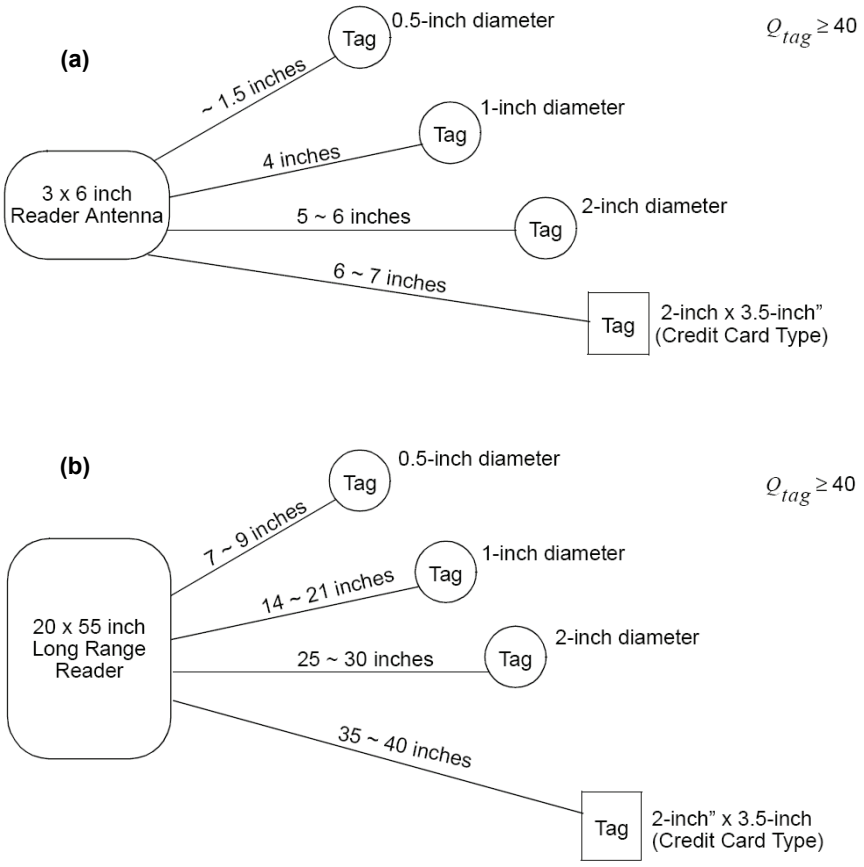

Figure 7.12 Read ranges vs. tag sizes for (a) proximity applications, and (b) long range applications.

7.5 Experiments

The Gen-1 prototype was tested using water and acid dropped on the electrode. Fig. 7.13 shows the detected frequency from a spectrum analyzer at a distance of 10cm using a 12×15-cm^2 reader antenna. The DC power at the reader was 8V, 350mA. The read frequencies were 7.28, 8.0 and 11.4 kHz for air, water and acid, respectively. The higher frequency of the acid indicates that the solution has lower impedance. The signal

was readable up to 13 cm as shown is Fig.7.14(b), however, with more noises compare to the signal at closer distance Fig.7.14(a). Longer read range can be achieved with higher power reader. However, it might not be practical for a portable reader running from batteries.

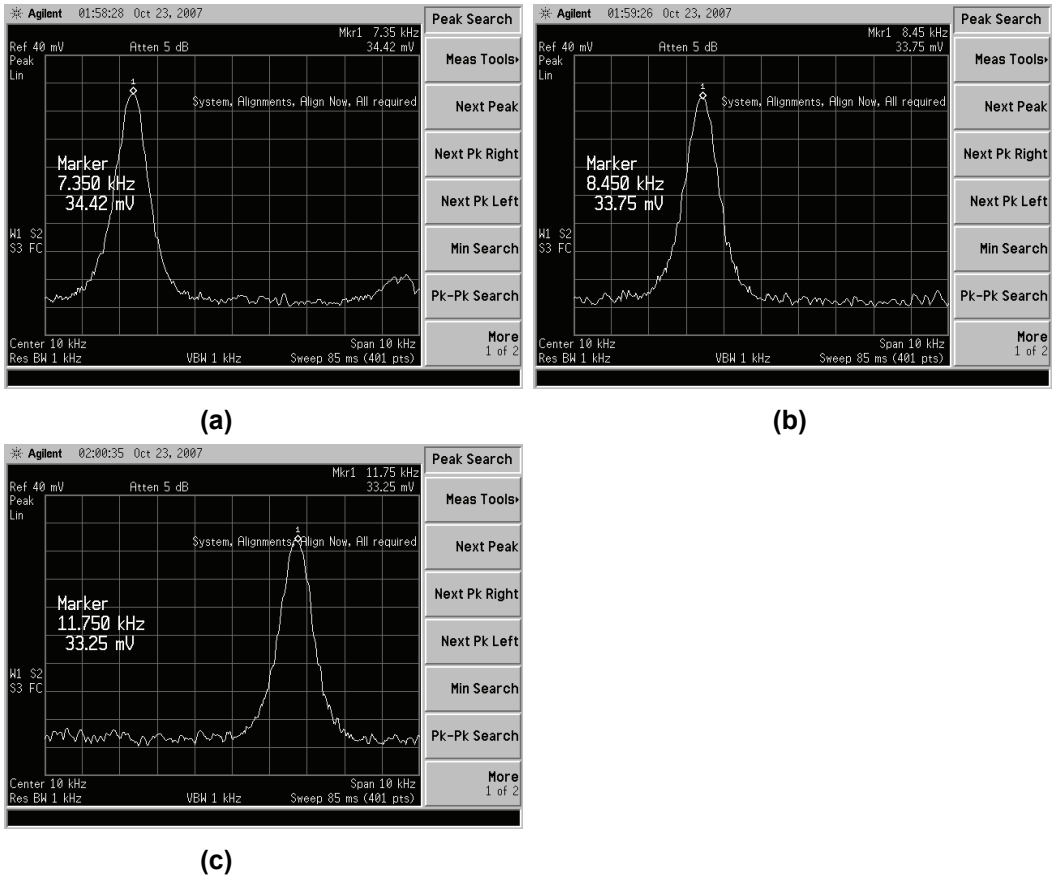

Figure 7.13 Detected signals from Gen-1 prototype at 10cm away from the reader antenna. The materials surrounding the electrode were (a) air, (b) water and (c) acid.

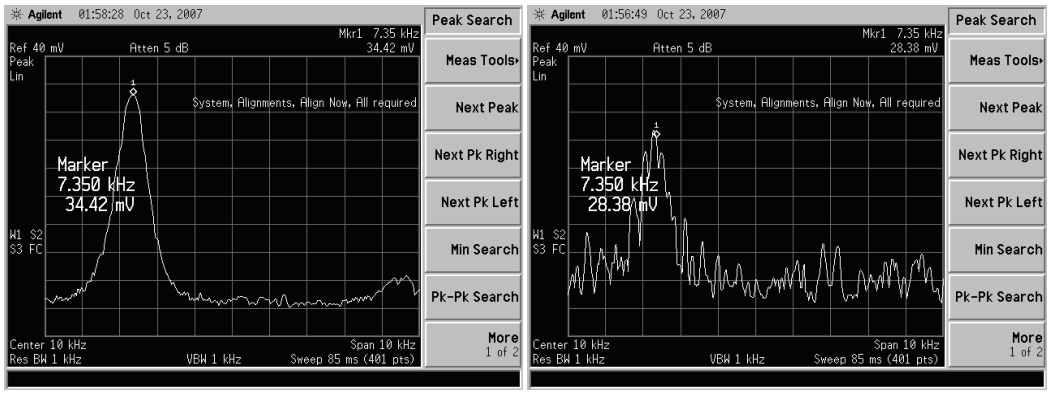

(a) **(b)**

Figure 7.14 Detected signals when the electrode is in air (a) at 10cm and (b) at 13 cm.

7.5.1 Animal testing

Dead pigs were used in our experiments. The first one was a female with the weight of 78lb and the chest perimeter of 70cm that died less than one hour previous to the experiment. The pig stomach was cut open and the Gen-1 impedance sensor was placed into the pig's esophagus 3-4 cm above the GE junction using an endoscope. The 12×15 cm^2 reader antenna was attached to the pig's skin outside the body. Several solutions were used to test the device including water, soft drink (Pepsi or Coke), orange juice with pulp (OJ(P)), orange juice with no pulp (OJ(N)), vinegar and simulated stomach acid. The solutions were flushed from the pig's mouth into the esophagus using a tube and a syringe pump. Although the stomach was cut open, the solution sometimes refluxed back onto the device. For this reason, each solution was pumped through the esophagus many times. This ensured that most of the liquid content at the electrode was testing solution. This is necessary to collect reliable data. Also,

water was flushed between the different solutions to clean the electrode and show the repeatability of the device. The device was first tested outside the pig's body. The read frequency was 7.3 kHz when the electrode was surrounded by air. The read frequencies in the esophagus are shown in Table 7.1.

Table 7.1 Read frequencies from the pig's esophagus with different flushed solutions.

No.	Solution	Frequency (kHz)	No.	Solution	Frequency (kHz)
1	None	8.78	10	OJ (N)	9.35
2	Water	8.28	11	OJ (N)	9.38
3	Water	8.15	12	Water	8.45
4	Pepsi	9.03	13	Vinegar	9.38
5	Pepsi	9.15	14	Vinegar	9.55
6	Water	8.48	15	Vinegar	9.36
7	OJ (P)	9.30	16	Water	8.6
8	OJ (P)	9.33	17	Acid	11.68
9	water	8.55	18	Acid	11.43

From the results the detected frequency increased immediately from 7.3 kHz to 8.78 kHz when the device was placed in the esophagus. This means the residue inside the esophagus has a lower impedance than that of air. When the water was pumped through the esophagus, the frequency was reduced from 8.78 kHz to about 8.2 kHz. This result suggested that the residue materials in the esophagus have lower impedance than that of water. In the next step, Pepsi was pumped in and the frequency increased to 9 kHz which showed the low impedance of the soft drink containing carbonic acid. For the

orange juice, both with pulp and without pulp gave the same frequencies around 9.3 kHz. This indicates low impedance involving the acidity of the solutions that is similar to the results from that of vinegar. The simulated stomached acid, which is known to be a strong acid, gave the highest frequency more than 11 kHz. This means that it has a very low impedance.

7.5.2 Performance comparison with BRAVO

Currently, BRAVO wireless pH sensors [7.16] are used in many hospitals. This unique implanted device is known to be the first comfortable and reliable acid reflux diagnosis method, in fact, the only available choice. It is therefore the best reference for our wireless impedance sensor to validate the results. Due to the long and narrow shape of the esophagus, another prototype that is more suitable to be implanted was made on a PCB with the size of 30×6 mm^2. The antenna was made from a magnet wire AWG32 winding around the PCB. The device was then conformally coated with PDMS as shown in Fig. 7.15 compared to BRAVO wireless pH capsule.

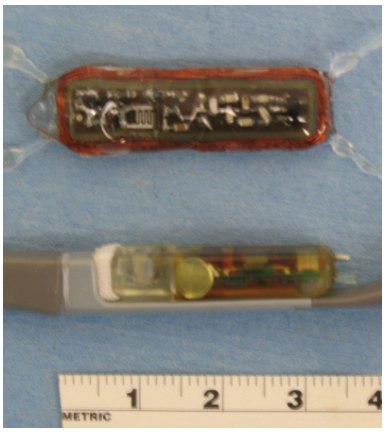

Figure 7.15 (a) The Gen-2 wireless impedance sensor prototype.
(b) BRAVO wireless pH capsule.

This new prototype will be referred as a Gen-2 wireless impedance sensor. Another dead pig was used for the experiment. A BRAVO capsule was tied up with the wireless impedance sensor using a suture wire. Both devices were placed in to the pig's esophagus and the experiment began with the same procedures explained previously. The pH results from BRAVO and the read frequencies from the impedance sensor were plotted in Fig. 7.16.

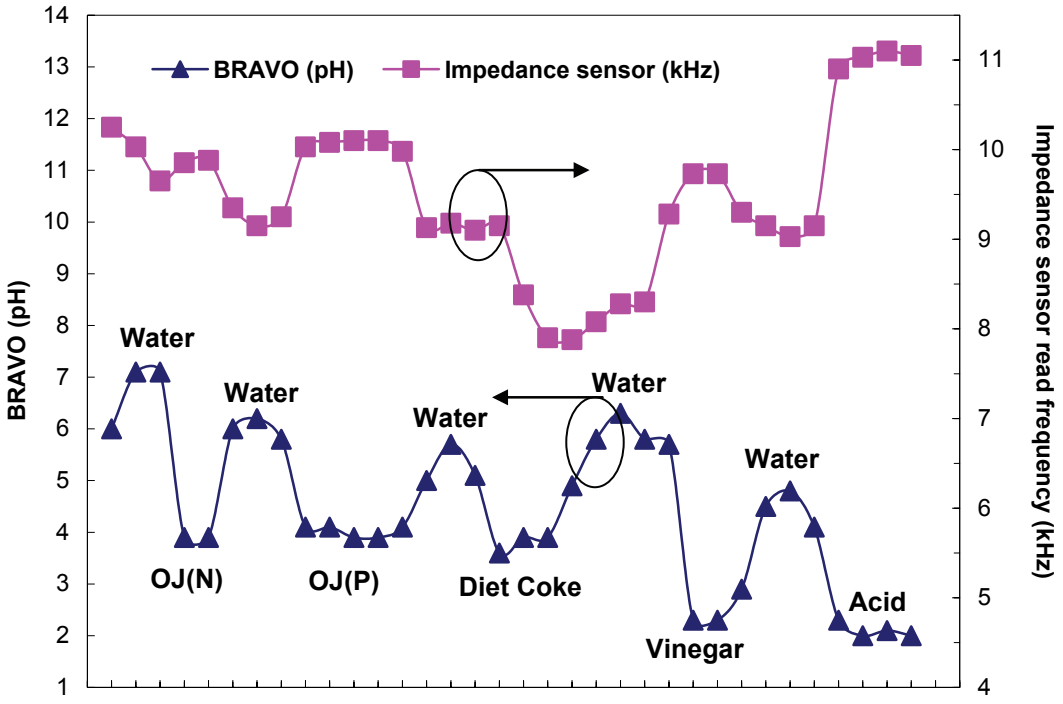

Figure 7.16 Read frequencies from the Gen-2 impedance sensor and pH values from BRAVO in the pig's esophagus.

In general, the measured frequency can be correlated to the pH changes. The fluctuation cycles of the frequencies between water and orange juice, vinegar or acid can be correlated with the pH changes. The pH changes from low to high corresponds to frequency changes from high to low and vice versa. The results from the soft drink,

however, were unusual. The frequencies from the Diet Coke were around 8 kHz while that of the water was around 9 kHz. This means the Diet Coke has higher impedance than that of the water. This is not true because the soft drink contain carbonic acid consisting of ions that lower the impedance. In fact, what happened in the experiment was that when the Diet Coke was pumped into the esophagus, a lot of bubbles were generated. The air bubbles occupied the surface area of the electrodes on the impedance sensor preventing the solution to make a good electrical contact with the electrode. The interdigited electrode used for the sensor has a conductor spacing less than 200 μm which is smaller than the size of most air bubbles. The sensor thus responded to air bubbles as a high impedance air reflux in stead of the Diet coke. These results suggest that the electrode shape needs to be considered in practice. Nevertheless, these results verify that the device can also detect air reflux while the pH sensor cannot.

For more accurate measurement, an in vitro experiment was conducted by placing both devices in beakers of different solutions. This way the devices were completely surrounded by the solutions. It was assured the two devices were in the same condition. The experiment was repeated again after one day for reliability matter. The results are shown in Fig. 7.17 where the 1st and the 2nd experiments are indicated by #1 and #2 respectively.

The results show very clear correlation between pH and measured frequencies in the same way of the previous experiments. This time, the frequency from the Diet Coke, however, was about 9.7 kHz higher that that of water. This is because there were fewer bubbles formed by dipping the device into the beaker than the bubbles that were

generated by using a syringe pump to flush the solutions. Nevertheless, the frequency could go beyond 10.5 kHz, showing lower impedance without the present of bubbles. In this experiment, the results from #1 and #2 show good repeatability and reliability for both devices. However the wireless impedance sensor performed better than BRAVO for the measurement of water which is a commonly know defect when using a pH sensor to measure a neutral solution or weak acid.

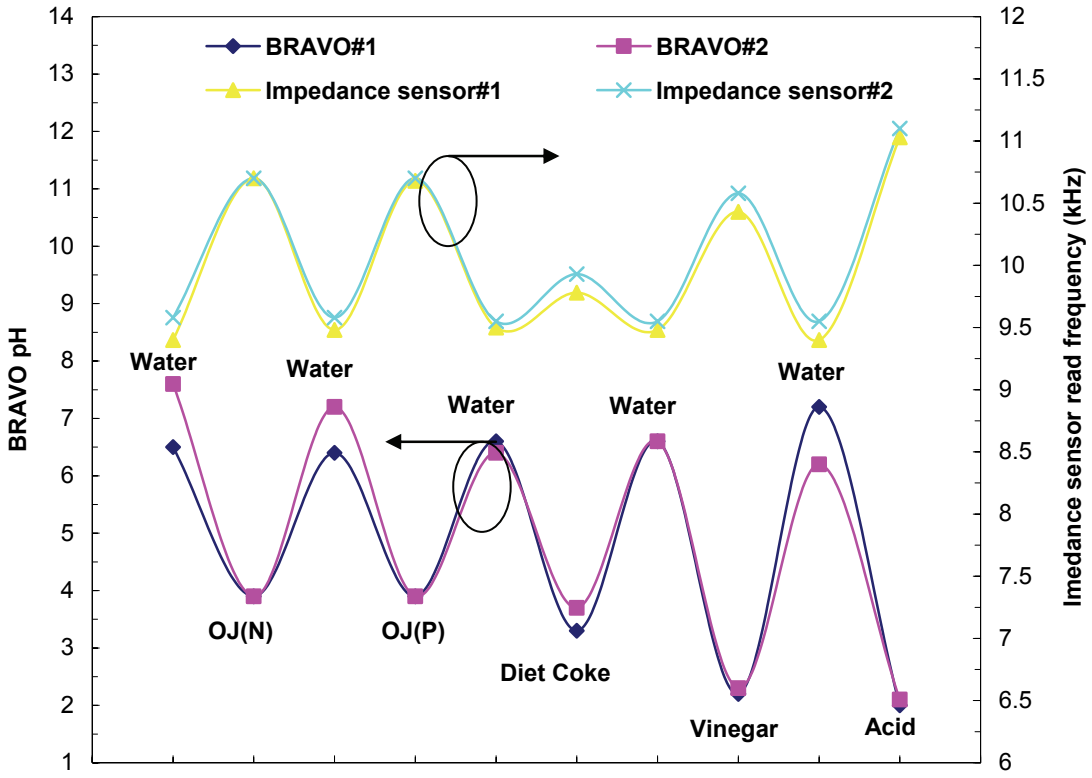

Figure 7.17 Read frequencies from the impedance sensor and the respective pH values from BRAVO. The experiments were conducted in beakers.

Another test was conducted in the 3rd pig with acid, salt and alkaline solutions flushed through the pig's esophagus to simulate the reflux to compare the wireless impedance sensor and the BRAVO wireless pH capsule. The results are shown in Fig. 7.18.

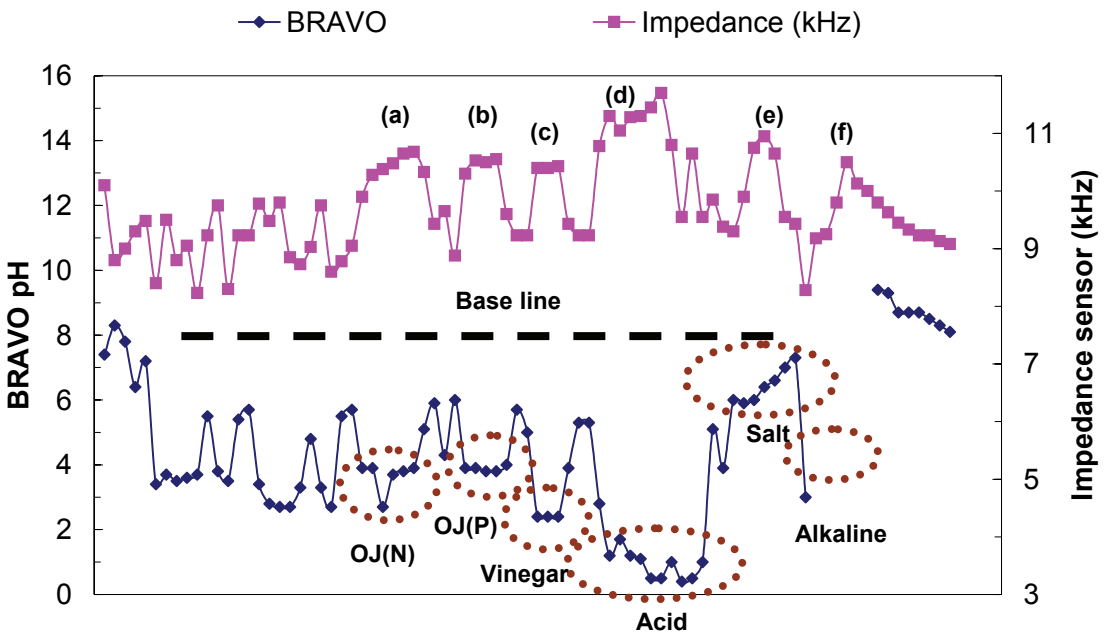

Figure 7.18 Results from the 3rd pig. The frequency peaks from the impedance sensor (a-f) are OJ(N), OJ(P), vinegar, acid, salt and alkaline solutions respectively.

The data shows that the pH dropped from the base line when there were acid refluxes caused from orange juice without pulp (OJ(N)), orange juice with pulp (OJ(P)), vinegar and acid solutions. The measured frequencies from the impedance sensor increased from the base line accordingly. The frequency peaks are indicated in Fig. 7.18(a-d) for OJ(N), OJ(P), vinegar and acid solutions respectively. Both impedance and pH sensors showed very high correlation. The results from the salt solution,

however, did not significantly change the value of pH from the BRAVO capsule. The impedance sensor, on the other hand, detected the salt reflux in the same manner of the acid reflux as the frequency increased noticeably from the base line (Fig. 7.18(e)). For the alkaline reflux, the BRAVO capsule indicated errors showing that the pH was too high while the impedance sensor gave high frequency measuring the low impedance of the alkaline solution (Fig. 7.18.(f)).

7.5.3 Impedance vs pH testing

To find out the relationship between the impedance and pH values of the solutions more experiments were conducted. The impedance sensor was placed in a beaker filled with water. Strong acid (HCL) and alkaline (KOH) solution were gradually added to increase or decrease the pH values of tab water (the tab water may not have the pH value at 7 due to impurities). A commercial pH sensor (HANNA Instruments) was used to measure the pH values correlated to the read frequencies from the wireless impedance sensor. The results are shown in Fig. 7.19(a) for acid and 7.19(b) for alkaline.

In both the acid and alkaline cases, the measured frequencies increased when more HCL of KOH solutions were added into the water. This is because both HCL or KOH create ions in water that reduced the impedance. Although the impedance sensor can sense the impedance changes, it could not distinguish between acid and alkaline with the same concentration. For impedance sensing, any solution with the same ion concentration will give the same results which are not related to the pH values. To verify this thought, the device was tested in salt solution by adding 25ml of typical salt

into 900ml of water. The pH of the water before adding salt was 8.71 and the read frequency was 9.48 kHz. After adding salt, the pH slightly changed to 8.77 while the frequency largely increased to 11.08 kHz similar to the number from strong acid or alkaline. It is conclude that the high frequency results from the impedance sensor do not necessary mean the solution is strong acid.

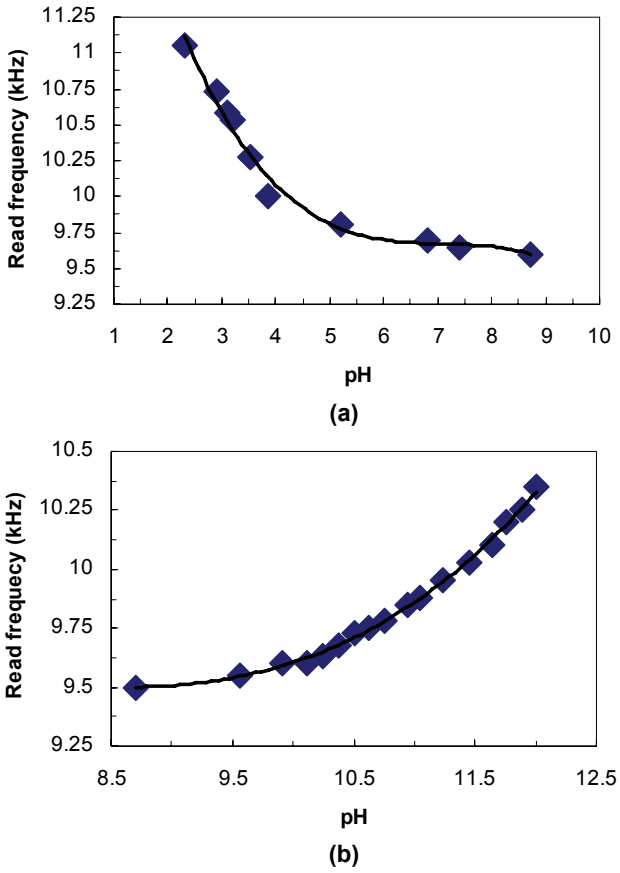

Figure 7.19 Read frequencies as a function of pH value for (a) acid. (b) alkaline.

However, it is unlikely that there will be alkaline reflux from the stomach often. For the purpose of reflux detection in the esophagus, the impedance sensor can detect

all kinds of reflux which usually involves acid or food residue. This could be an advantage over the pH sensor to encounter the diseases involving non-acid reflux. The impedance sensing is thus still suitable for this application, however, with some limitations.

7.6 Further modification of the wireless impedance sensor

So far, the experimental results show satisfied performance of our wireless impedance sensor. However, the size of the device is still quite large, making it uncomfortable when using it in a human esophagus. The size of the device was thus minimized to be comparable to the commercial BRAVO pH sensor. The smaller device provided less space for the antenna and degraded both power coupling and modulation efficiency. The major challenges were to provide enough power to operate the circuitry and to generate strong modulation signals from a small antenna. These were done using components with lower power consumption and some modifications of the circuit to achieve the same or better performance compared to that of the larger antenna.

The new design operated at 2V using a regulator S-817A20ANB from Seiko Instruments. The low voltage operation enabled the longer read range with the same power provided by the reader. A comparator TLV3012 (Texas Instrument) was chosen for the frequency generator because of its ultra low power consumption and its small size. Another suitable IC is the TLV3491 which consumes less power, but occupies more area. Both frequency generator and the modulator circuitry were modified. The frequency generator in Fig. 7.6, the resistors R_1, R_2, R_3, R_A, R_B and the capacitor C_1 had value of of 1MΩ, 1MΩ, 1MΩ, 12kΩ, 10kΩ and 2.2nF respectively in this new design.

The value of R_1 in the Gen-1 and Gen-2 prototypes was 10MΩ keeping the modulation at a low duty cycle to conserve the power for the LPV321 during the modulation. The new IC TLV3012, however, consumed a lot less power than that of LPV321, and thus the modulation can be done at a higher duty cycle. The 1MΩ value of R_1, R_2, R_3 were selected resulting in 50% duty cycle at the output frequency. This output signal turned the modulator on for a longer period of time and gave stronger signals that would be detected by the reader compared to the first design.

For the modulator, the Gen-1 and Gen-2 design in Fig. 7.7 included a transistor M_2 used to turn off the modulation when the DC voltage from the regulator was too low. This gave the storage capacitor more time to harvest the power from the reader. In this new design, the power consumption of the circuit was much lower and the regulator provided a V_{CC} of 2V closed to the threshold voltage of the modulation transistor. The voltage of lower than 2V can hardly operate both M_1 and TLV3012 and thus the modulation cannot occur. Moreover, the read range was limited by noise in the environment and the sensitivity of the reader instead of power constraint. The use of M_2 was therefore no longer necessary and was removed from the circuit. A coil antenna was made using AWG34 magnet wire. This latest prototype will be referred as Gen-3 wireless impedance sensor. The complete circuit diagram of the Gen-3 transponder is shown in Fig. 7.20 with the device photograph in Fig. 7.21 compared with a BRAVO capsule.

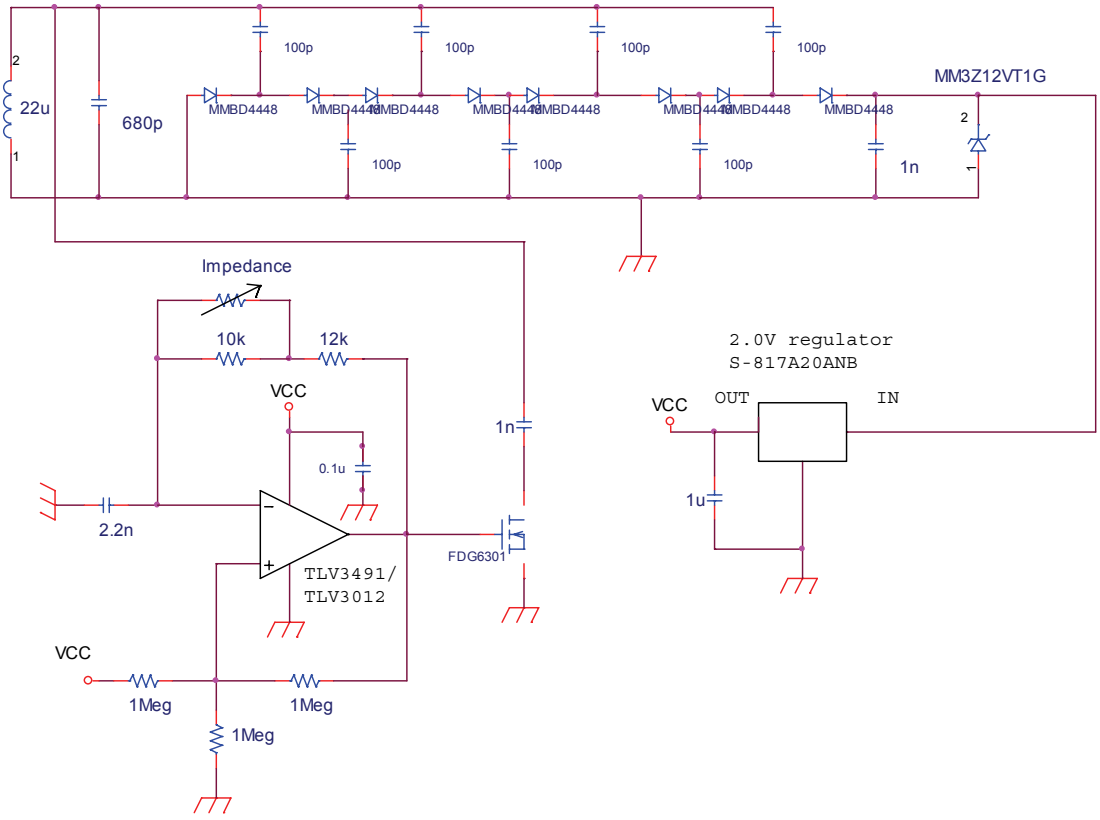

Figure 7.20 The Gen-3 transponder circuit diagrams.

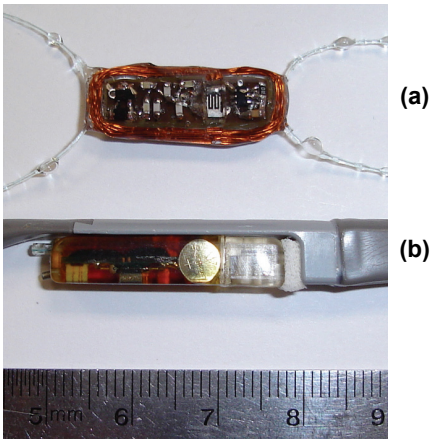

Figure 7.21 (a) The Gen-3 wireless impedance sensor prototype (b) BRAVO wireless pH capsule.

The Gen-3 sensor was tested using water and acid dropped on the electrode. The reader antenna was 9×12 cm with the DC supply of 8V 400mA. The results are shown in Fig. 7.22.

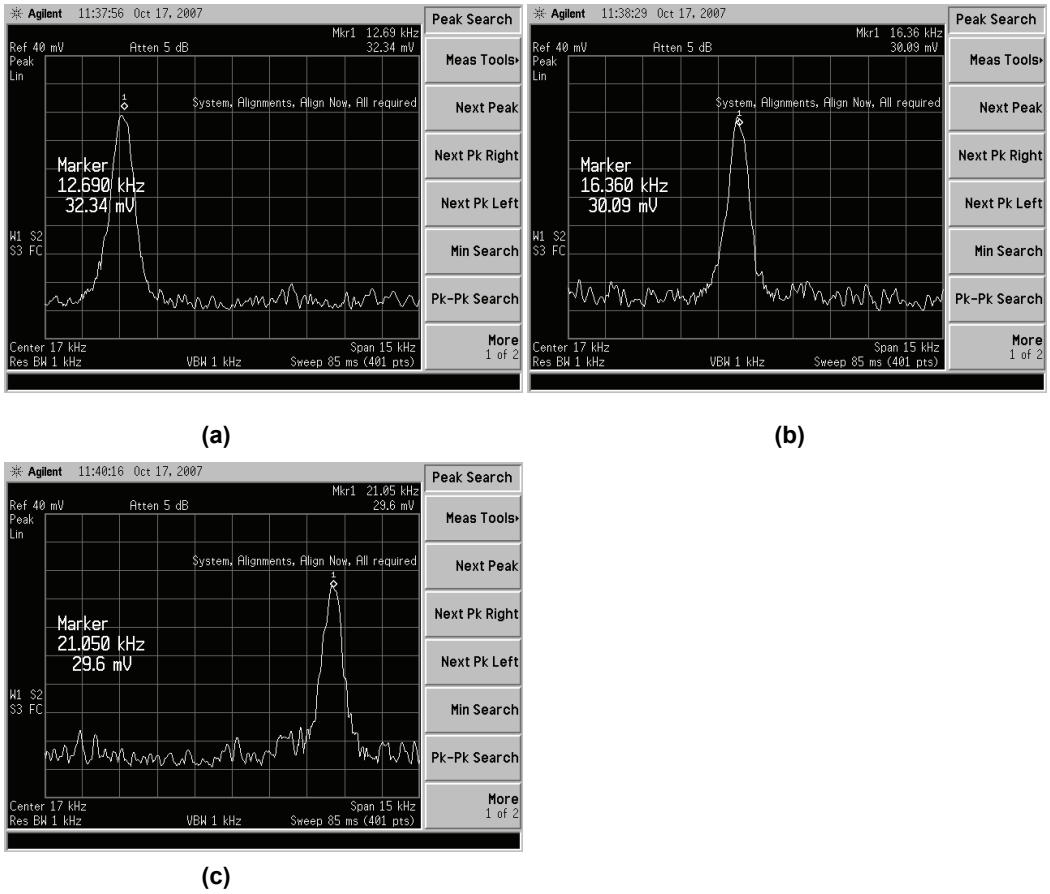

Figure 7.22 Detected signals from Gen-3 prototype at 10cm away from the reader antenna. The materials surrounding the electrode were (a) air, (b) water and (c) acid.

The test results show the measured frequencies of 12.7kH, 16kHz and 21kHz in air, water and acid respectively at 10cm away from the reader. The signal quality is comparable to those of the Gen-1 prototype in Fig. 7.13 with more than 50% less volume and twice the frequency difference from water to acid thereby giving higher

sensitivity. The signal is sill readable at 12cm away from the reader as shown in Fig. 7.23(b) however, with more noises compare to the signal at closer distance Fig.7.23(a). The Gen-3 transponder also has comparable read range to a typical RFID tag as shown in Fig. 7.12(a). While the typical RFID tag with the size of 1" in diameter can be read at 4" from the 3"×6" antenna, the developed transponder achieved the same range with smaller transponder size and smaller reader antenna.

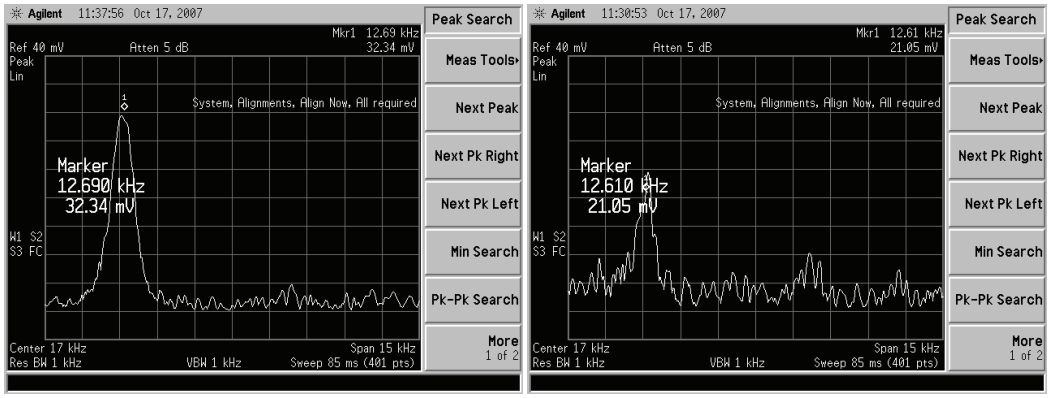

(a) **(b)**

Figure 7.23 Detected signals when the electrode is in air (a) at 10cm and (b) at 12 cm.

CHAPTER 8

A COMBINE WIRELESS IMPEDANCE/PH SENSOR FOR DETECTING GASTROESOPHAGEAL REFLUX

Although the wireless impedance sensing that can detect the reflux was achieved, the impedance vs pH testing results showed that, in certain cases, the impedance sensor cannot verify the acidity of the reflux which is usually an indicator of the severity of the symptom. It is always better to have the pH information of the reflux as well. This can be done by combining both sensors together in the same device.

8.1 Wireless batteryless pH sensor

The transponder architecture developed for the impedance sensor can be easily applied to the pH sensor. The only modification needed is the interface between the sensor and the frequency generator. Currently the pH sensing mechanisms commonly rely on the differential voltage generated from the chemical reaction between hydrogen ions and special electrodes. To transform the voltage to frequency signal for our wireless sensing configuration, some modulation of the frequency generator is needed.

The square wave signal generated from the relaxation oscillator is based on the voltage level at the input of the comparator [8.1]. The shift in the voltage at the non-inverting input of the comparator can also change the output frequency. By replacing the ground at the R_2 of the circuit in Fig 7.6 to the sensing voltage from the pH sensor,

the frequency generator can be used to transfer the voltage changes to frequency variation which can be detected wirelessly using the same reader previously designed. In this work, a pH sensor based on IrOx electrodes was used [8.2]. The sensor generates a voltage in the range of -0.1 to +0.5V for the pH sensing range from 2-12. A new frequency generator was designed to integrate this with the pH sensor as shown in Fig. 8.1. A op-amp (OPA349, Texas Instrument) is used as a buffer for the pH sensor. The 1MΩ resistor and the 100pF capacitor were added to keep the voltage between -0.1 to +0.5V from the pH sensor stable.

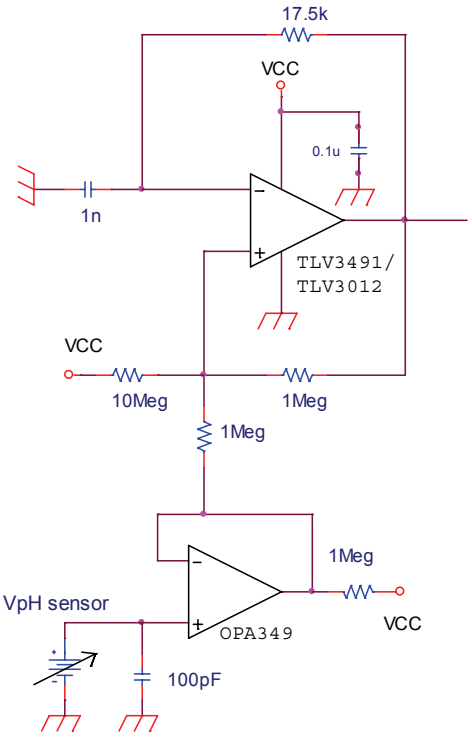

Figure 8.1 Frequency generator circuit diagram for pH sensor.

The circuit was made on a breadboard using adapters to insert the SMD packaged ICs into the socket. The results are shown in Fig. 8.2. When the pH decreased

toward acid, the sensor generated higher voltage. The measured frequency thus decreased approximately from 22kHz to 17kHz for the pH of 2 to 12, respectively. The new frequency generator transduced the voltage to a frequency with linearity similar to the pH sensor voltage. Thus the wireless batteryless pH sensor was achieved. The circuit components can be assembled on a PCB board with PDMS coated as it was done for the impedance sensor.

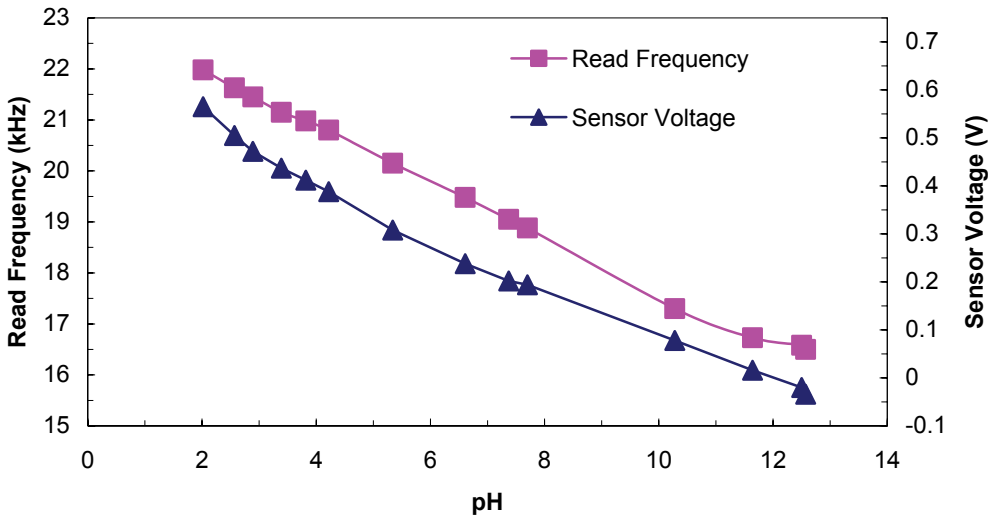

Figure 8.2 Read frequency and sensor voltage as a function of pH.

8.2 Technique to read from two sensors

As discussed in chapter 7.5.3, the data from an impedance sensor may not be sufficient to diagnose specific diseases. It is more beneficial to collect both pH and impedance data in the esophagus to analyze complex symptoms. However, techniques to measure both data together are needed. These techniques can be applied to measured data from more than two sensors as well. In general, there are two approaches to collect

2 sensing quantities from the sensors in the esophagus to collect the data from sensors. The techniques can be summarized in Table 8.1.

Table 8.1 Techniques to read data wirelessly from two sensors

No. of transponder (No. of Antenna)	No. of Carrier frequency	No. of frequency generator for sensor in each transponder
2	1	1
	2	1
1	1	2
	1	1

8.2.1 Two transponders using the same carrier frequency

The easiest way to collect the impedance and the pH values is to put both sensors in the esophagus and read the data from both sensors at the same time. Each sensor needs to have its own antenna and circuitry and must be in the read range of the antenna. There is no modification needed at the reader. Although both sensors can receive power from the same carrier frequency from the reader, each sensor has to modulate the data with different frequency ranges to avoid the ambiguity at the reader. This can be done by changing the resistors and the capacitor in the frequency generator circuit to create different output frequencies. Fig. 8.3 shows the results using this approach.

The 1st sensor modulated at 7.04kHz and the 2nd sensor at 11.28kHz. Fig 8.3(a,b) shows the individual reading signal from the sensors. When both sensors were placed

next to each other, the reader read both frequencies as shown in Fig. 8.3(c). The results show that, when both sensors were in the same reading range of the reader, both signals were detected. However, because they used the same carrier frequency, the signals became noise to each other making the SNR dropped dramatically.

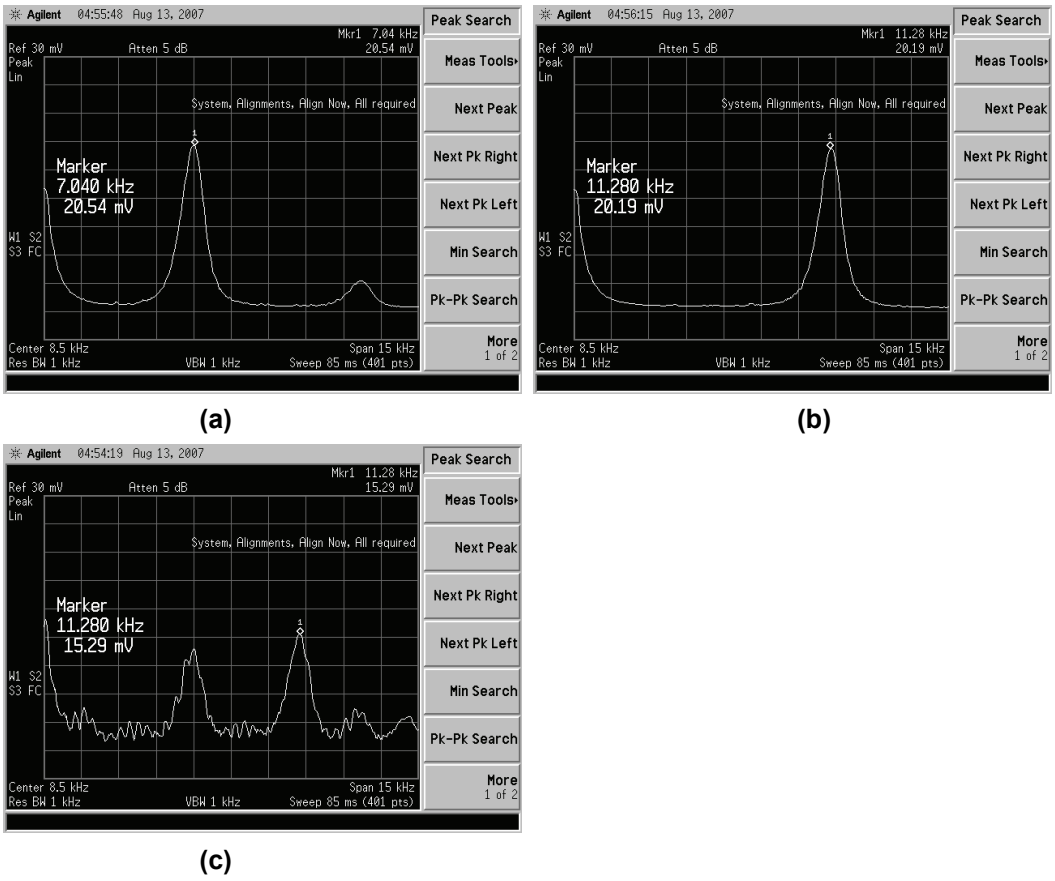

Figure 8.3 Two transponder using same carrier frequency. (a) Individual read frequency from the 1st transponder. (b) Individual read frequency from the 2nd transponder. (c) Reader frequencies from both transponders.

8.2.2 Two transponders using different carrier frequencies

Knowing that the communication of the sensor and the reader relies on the resonance frequency of LC circuit, both sensor and reader will not responses to the signal in other ranges. Thus different carrier frequencies can be used to avoid the interference between sensors and both sensors can share the same modulated frequencies as well. At the sensor, the LC resonance circuit is needed to be modified while the rest of the transponder circuitry can be kept the same. The signals from the sensors can be read from either of the two separated readers operating at different carrier frequencies or from one reader that can switch between the frequencies. A reader with the antenna inductance of 17μH (L_2 in Fig. 7.9) was used. The resonant capacitor on the reader (C_2 in Fig. 7.9) was changed from 800pF to 2800pF to switch the carrier frequency from 1.315MHz to 0.755MHz respectively. Fig 8.4 shows the detected signals from the 2 transponders with the configuration in Table 8.2.

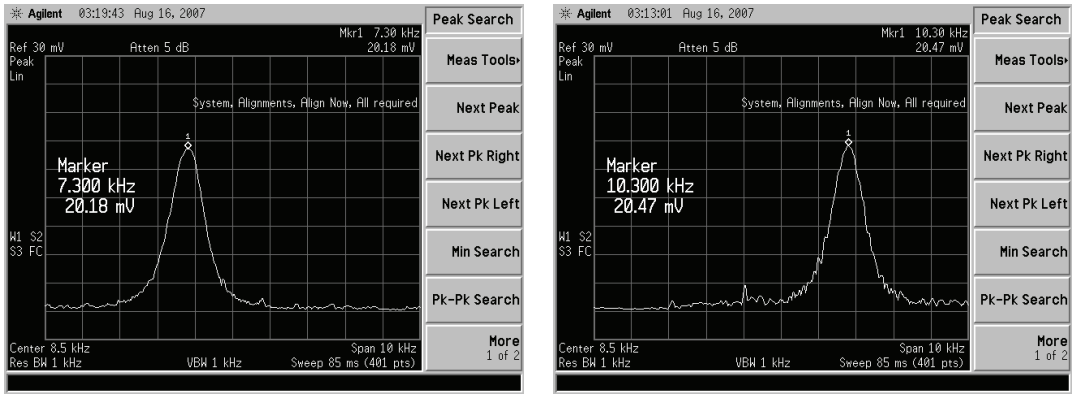

(a) **(b)**

Figure 8.4 Detected signal from 2 transponders with different carrier frequencies.

Table 8.2 Configuration for the transponders and the reader.

No.	Antenna Inductance	Resonance Capacitor	Carrier Frequency	Modulated Frequency
Transponder#1	16μH	1nF	1.315MHz	7.3kHz
Transponder#2	32.79μH	1.94nF	0.755MHz	10.3kHz

The results show that there was no interference between each signal when different carrier frequencies were used. Moreover, the same range of the modulated frequencies can be used because each signal will be read at different time or by different readers. The carrier frequencies of 1.315MHz and 0.755MHz were chosen to ensure that the interference was minimized. However, the bandwidth was large. Smaller frequency separation can be used for a high Q circuit which is suitable for the system with a high carrier frequency.

8.2.3 Single transponder with separate frequency generator for each sensor

To read the data from multiple sensors, it is preferable to have only one implant connected with different sensors. This way the size of the implant can be minimized assuming that the circuit size is smaller than that of the antenna. The data can be modulated using various multiplexing techniques. However, the system was design to be simple and with no processing capability. A simple time division multiplexing (TDMA) scheme will be considered. For two sensors, two frequency generators can be used in a transponder. Each of them generates different frequency ranges from each sensor. The TDMA can be realized using an SPDT switch (TS5A3159a, Texas instrument) to multiplex each sensor signal to the modulation transistor. Another

frequency generator is used to control the SPDT switch. This control signal can be adjusted to satisfy the required sampling rate needed for the monitoring. The diagram of this approach is shown in Fig. 8.5. The circuit was assembled on a breadboard using variable resistor to emulate an impedance sensor and DC source to emulate a pH sensor. The frequencies vary between 6.88 to 18.88 kHz for the impedance sensor and from 21.28 to 25.7 kHz for the pH sensor. The results are shown in Fig. 8.6.

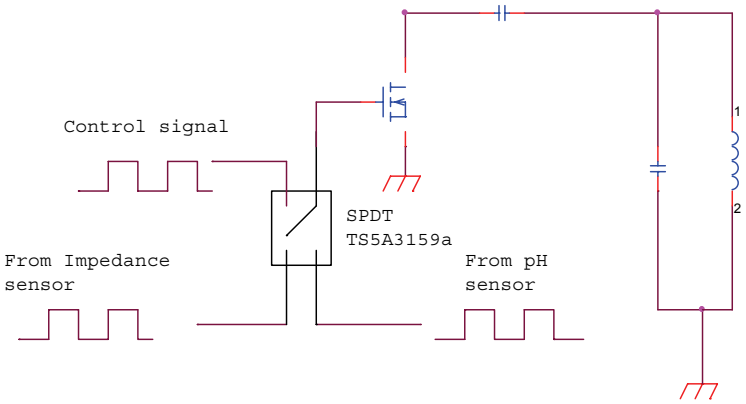

Figure 8.5 Configuration for the single transponder approach.

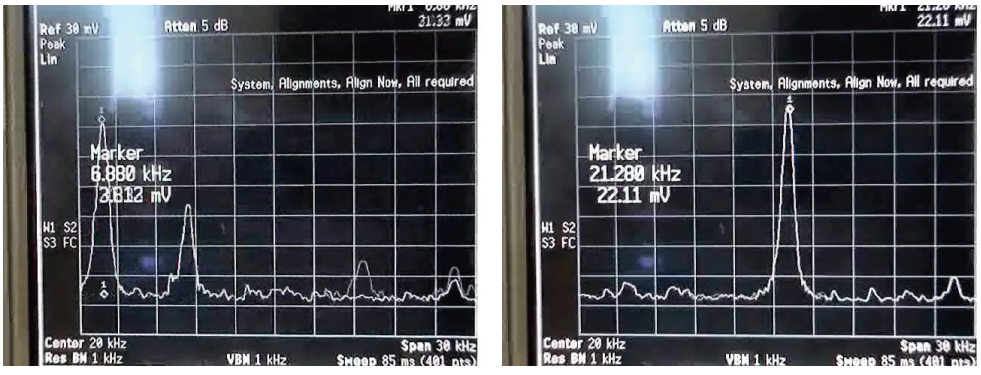

(a) (b)

Figure 8.6 Read frequencies when the switch connected to (a) impedance sensor and (b) pH sensor.

8.2.4 Single transponder with the same frequency generator for each sensor

Another way to collect the data from both sensors is to use switches to multiplex the sensor itself directly. This can be done using two SPDT switches. A possible circuit topology is shown in Fig. 8.7.

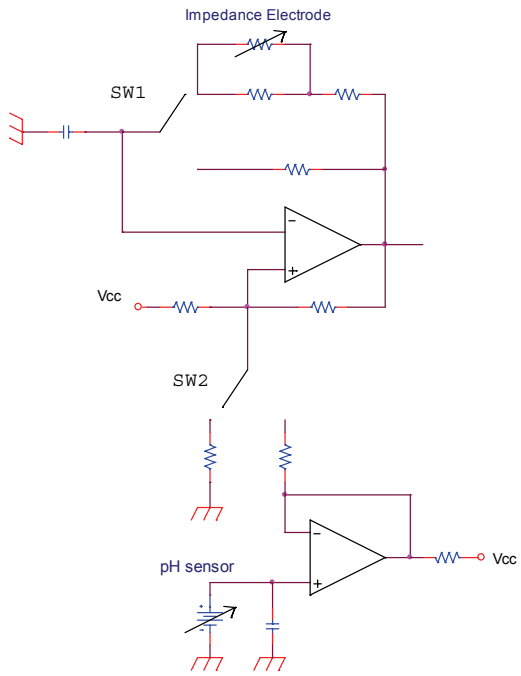

Figure 8.7 A possible circuit topology for an integrated impedance and pH sensor.

When both switches are OFF, the frequency generator connects to the impedance electrode and produces the output frequency for the impedance measurement. When both switches are ON, the circuit generates the frequency from the pH sensor. This method reduces the number of components required to achieve multiple sensors measurement. However due to the non-ideal characteristic of the switches, the currents and voltages in the oscillator circuits will be affected. Carefully adjustment and

calibration will be needed to overcome the output frequency shifts that may occurre from the non-ideal switches. Using the TS5A3159a in the frequency generator, the output frequency increased more than 20 kHz from the original frequency of 10 kHz.

8.3 Summary

The wireless batteryless sensors for gastroesophageal reflux diagnosis that can be used for long term monitoring have been demonstrated. The impedance or pH of the reflux can be determined using similar circuitry. Using typical SMD packaged components, the device can be as small as the commercially available battery powered sensors. Both sensors can be combined to collect data from multiple sensors for better performance that can encounter complex symptoms. The size of the circuitry can be minimized using small IC packages or a custom made ASIC (application specific IC) chip.

CHAPTER 9

CONCLUSIONS AND FUTURE WORK

9.1 Conclusions

In this dissertation, two medical applications using wireless devices have been investigated. In the fist application, a system that can wirelessly activate brain stimulation to reduce pain when the wirelessly recorded signals from a neuron indicate certain pain level was proposed. The prototype was designed, fabricated and tested in vivo with anesthetized rats. The device is small enough to be implemented in freely moving animals. The results show the inhibition of action potentials from the spinal cord that eliminates the communication to the brain and therefore reduces the sensation of pain. The system includes a feedback function that has been tested to automatically activate the brain stimulation. The device can be used with a different kinds of electrodes. The optimized recording and stimulating positions as well as stimulating parameters can be investigated using this prototype. The design methodology could also be used in other applications that require neural recording and a stimulating system.

In the second application, wireless sensors for gastroesophageal reflux diagnosis have been designed, fabricated and validated. The proposed approaches are based on impedance measurement that can detect both acid and non-acid reflux. The design for both amplitude detection and frequency detection are proposed. The frequency

detection approach showed better performance of longer read range and more reliable data that is independent on the reading position. The prototype of the impedance sensor can be as small as the commercially available battery powered wireless pH capsule. The device was tested in a dead animal showing the capability of using it on humans. The results show comparable performance to the commercial pH sensors to detect acid reflux. The device can be used for long term monitoring of both acid and non-acid reflux as well. A wireless batteryless pH sensor using a similar design was also proposed. The techniques to collect the data from both a pH sensor and an impedance sensor were investigated. This enables the ultimate device for gastroesophageal reflux monitoring that can detect any reflux and quantify the pH values to analyze complicated diseases. The design methodology of this wireless batteryless sensor could be easily adapted to any other resistive, capacitive or voltage based sensors that can be deployed in many other monitoring needed in human body.

9.2 Future works

For the pain management application, the future work will be focused on the experiment that uses a freely moving animal. Finding the best way to evaluate the pain from neural signals and optimizing the parameters of brain stimulation for pain relief will be the next step. The device will be used to record neural signals to correlate with pain, for example, by recording the signal before and after giving the pain or injury to the animals. The device will also be used to apply the stimulation to investigate the efficiency of pain relief. This can be done by observing the animal behavior

corresponding to the stimulation. The animal behavior caused from the stimulation can be compared with other pain relief methods to evaluate the efficiency of the parameters.

For the gastroesophageal reflux monitoring, one of the improvement needed is to make the sensor more sensitive to the material with the pH more than 4 to compensate the deficiency of the pH sensor. This can be done by designing to the electrodes with fine fingers to increase the capacitance changes from the materials with small number of ions. The next step could be the miniaturization of the circuitry by using a custom ASIC chip. The small size of the chip allows the integration of multiple sensors or arrays that can be put along the esophagus to evaluate the volume and the direction of the reflux episodes. The data collection could contain identification number as in RFID tags to provide the details of the implant positions and the patient information. Another focus could be on the read range. This can be improved by using lower power circuitry, better quality factor of the antenna and higher sensitivity of the reader. Digital modulation could be used to provide better SNR achieving longer read range. The transponder circuit design can be used with different sensors that are based on resistive, capacitive or voltage variation to monitor the needed conditions in human body. Simple demonstrations are shown in Fig. 9.1 by replacing the impedance electrode of the transponder with a thermistor and a force sensitive resistor to achieve a temperature sensor and a pressure sensor respectively. The device characterization and packaging are needed to be investigated for specific applications.

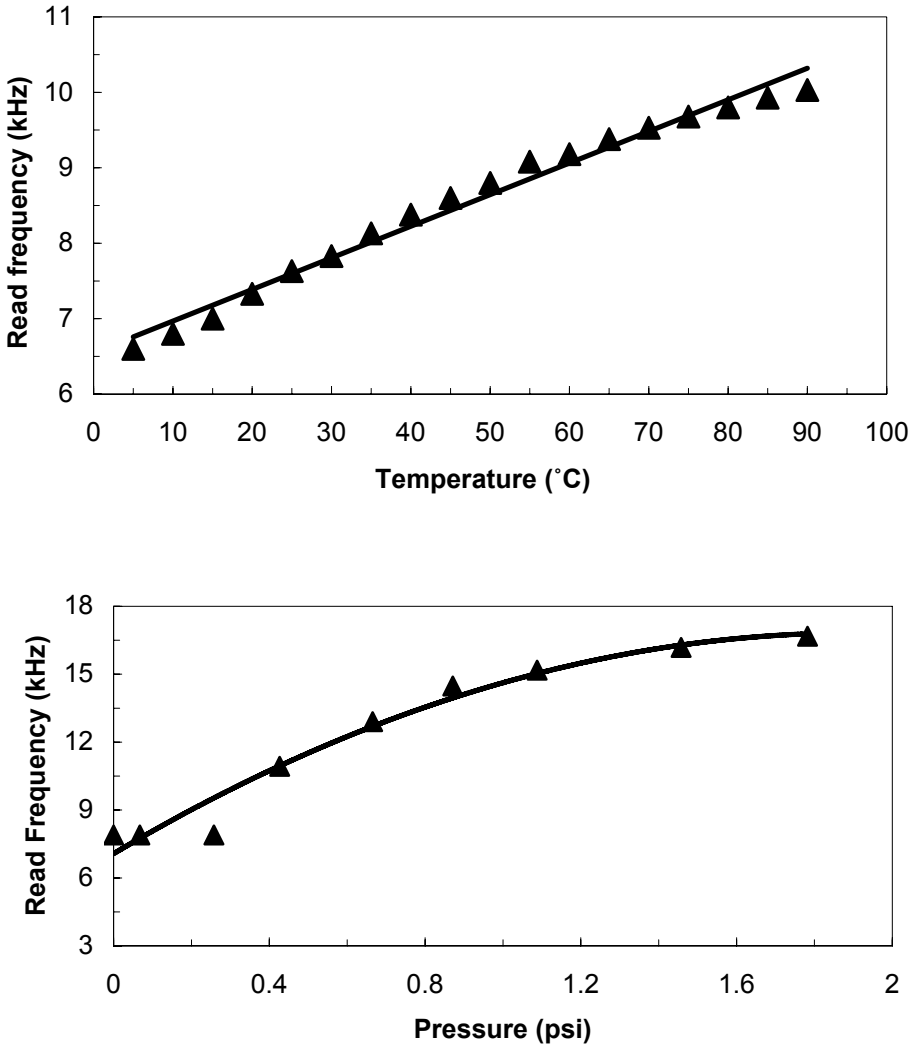

Figure 9.1 Read frequencies from wireless batteryless transponder. (a) Temperature sensor. (b) Pressure sensor.

REFERENCES

[2.1] Medical Data International, Market and Technology Reports, U.S. Markets For Pain Management Products, Report RP-821922, June 1999.

[2.2] J. Reggia, E. Ruppin, R. Berndt, Neural Modeling of Brain and Cognitive Disorders, World Scientific: Singapore, 1996.

[2.3] ABV. Apkarian, SN. Ayrapetian, Pain Mechanisms and Management, IOS Press, 1997.

[2.4] K. McCormack, "Signal transduction in neuropathic pain, with special emphasis on the analgesic role of opioids - Part I: The basic science of phenotype expression in normal and regenerating nerves," *Pain Reviews*, Vol.6, pp.3-33, 1999.

[2.5] LH. Finkel, "Neuroengineering models of brain disease," *Annual Review of Biomedical Engineering*, Vol.2, pp.577-606, 2000.

[2.6] H. Fields, J. Levine, "Pain-Mechanisms and Management," *West J Med*, Vol. 141, pp. 347-357, 1984.

[2.7] R. North et al., "Failed back surgery syndrome: 5-year follow-up after spinal cord stimulator implantation," *J. Neurosurg*, Vol.28, pp.692-699, 1991.

[2.8] R. North et al., "Spinal cord stimulation for chronic, intractable pain: experience over two decades," *J Neurosurg*, Vol. 32(3), pp.384-395, 1993.

[2.9] K. Burchiel et al., “Prospective, multicenter study of spinal cord stimulation for relief of chronic back and extremity pain,” *Spine*, Vol. 21,pp.2786-2794, 1996.

[2.10] T. Cameron, “Safety and efficacy of spinal cord stimulation for the treatment of chronic pain: a 20-year literature review,” *J. Neurosurg: (Spine 3),* Vol.100,pp.254-67, 2004.

[2.11] K. Wise, D. Anderson, J. Hetke, D. Kipke, K. Najafi, “Wireless implantable microsystems: high-density electronic interfaces to the nervous system,” *Proc. IEEE*, Vol.92(1), pp.76-97, 2004.

[2.12] E. Kandel, J. Schwartz, T. Jessell, Principles of neural science, New York: McGraw-Hill; 2000.

[2.13] M. Hughes, D. Banks, D. Ewins, “Action potential velocity detection using a penetrating microprobe,” *Measurement Science and Technology*, Vol.16(3)3, pp.N7-N10(1), 2005.

[2.14] http://en.wikipedia.org/wiki/Action_potential

[2.15] I. Obeid, M. Nicolelis, P. Wolf, “A multichannel telemetry system for single unit neural recordings,” *J Neurosci Methods*, Vol.133, pp.33-38, 2004.

[2.16] C.-W. Peng, J.-J. Chen, C.-C. Lin. P. Poon, C.-K. Liang, K.-P. Lin, “High frequency block of selected axons using an implantable microstimulator,” *J Neurosci Methods*, Vol.134, pp.81-90, 2004.

[2.17] A. Nieder, “Miniature stereo radio transmitter for simultaneous recording of multiple single-neuron signals from behaving owls,” *J Neurosci Methods*, Vol.101, pp.157-164, 2000.

[2.18] C.-N. Chien, F.-S. Jaw, “Miniature telemetry system for the recording of action and field potentials,” *J Neurosci Method*, Vol.147,pp.68-73, 2005.

[2.19] S. Schregardus, W. Pieneman, A. Maat, R. Jansen, T. Brouwer, M. Gahr, “A lightweight telemetry system for recording neuronal activity in freely behaving small animals,” *J Neurosci Methods*, Vol.155, pp.62-71, 2006.

[2.20] ES. Hawley, EL. Hargreaves, JL. Kubie, B. Rivard, RU. Muller, “Telemetry system for reliable recording of action potentials from freely moving rats,” *Hippocampus*, Vol.12, pp.505-513, 2002.

[2.21] S. Xu, SK. Talwar, ES. Hawley, L. Li, JK. Chapin, “A multi-channel telemetry system for brain microstimulation in freely roaming animals,” *J Neurosci Methods*, Vol.133, pp.57-63, 2004.

[3.1] S. Martinoia, M. Bove, G. Carlini, C. Ciccarelli, M. Grattarola, C. Storment, G. Kovacs, “A general-purpose system for long-term recording from a microelectrode array coupled to excitable cells,” *J. Neurosci Methods*, Vol.48, pp.115-121, 1993.

[3.2] LA. Geddes, Electrodes and the measurement of bioelectric events, Wiley-Interscience: New York, 1972:39-43.

[3.3] ES. Hawley, EL. Hargreaves, JL. Kubie, B. Rivard, RU. Muller, “Telemetry system for reliable recording of action potentials from freely moving rats,” *Hippocampus*, Vol.12, pp.505-513, 2002.

[3.4] C. Kitchin, L. Counts, A Designer’s Guide to Instrumentation Amplifiers, third ed., Analog device Inc., 2006.

[3.5] G. Wrobel, Y. Zhang, HJ. Krause, N. Wolters, F. Sommerhage, A. Offenhäusser, "Influence of the first amplifier stage in MEA systems on extracellular signal shapes," *Biosensors and Bioelectronics*, Vol.22, pp.1092-1096, 2007.

[3.6] B. Carter, Filter design in thirty seconds, application report, SLOA093: Texas Instrument Inc.; 2001.

[3.7] S. Xu, SK. Talwar, ES. Hawley, L. Li, JK. Chapin, "A multi-channel telemetry system for brain microstimulation in freely roaming animals," *J Neurosci Methods*, Vol.133, pp.57-63, 2004.

[4.1] M. Zimmermann, "Ethical guidelines for investigations of experimental pain in conscious animals [editorial]," *Pain*, Vol.16, pp.109-110, 1983.

[4.2] E. Kandel, J. Schwartz, T. Jessell, Principles of neural science, New York: McGraw-Hill; 2000.

[4.3] JM. Chung, DJ. Surmeier, KH. Lee, LS. Sorkin, CN. Honda, Y. Tsong, WD. Willis, "Classification of primate spinothalamic and somatosensory thalamic neurons based on cluster analysis," *J. Neurophysiol.*, Vol.56, pp.308-327, 1986.

[4.4] YB. Peng, Q. Lin, WD. Willis, "The role of 5-HT3 receptors in periaqueductal gray-induced inhibition of nociceptive dorsal horn neurons in rats," *J Pharmacol and Exp*, Vol.276, pp.116-124, 1996.

[4.5] AK. Senapati, SC. LaGraize, PJ. Huntington, HD. Wilson, PN. Fuchs, YB. Peng, "Electrical stimulation of the anterior cingulate cortex reduces responses of rat dorsal horn neurons to mechanical stimuli," *J Neurophysiol*, Vol.94, pp.845-851, 2005.

[4.6] G. Paxinos, C. Watson, The Rat Brain in Stereotaxic Coordinates, Academic Press: San Diego; 1998.

[4.7] L. McLean. R. Scott, P. Parker, "Stimulus artifact reduction in evoked potential measurements," *Arch Phys Med Rehabil*, Vol.77(12), pp1286-1292, 1996.

[5.1] T. Starner and D. Ashbrook, "Augmenting a pH medical study with wearable video for treatment of GERD," *IEEE Eighth International Symposium on Wearable Computers ISWC 2004*, Vol.1, pp.194-195, 2004.

[5.2] W. Faloon, "The hidden cancer epidemic," *Life Extension Magazine*, February 2003.

[5.3] P. Kahrilas, "Surgical therapy for reflux disease," *The Journal of the American Medical Association, JAMA.*, Vol.285(18), pp.2376-2378, 2001.

[5.4] M. Vincent, A. Robbins, S. Spechler, R. Schwartz, W. Doos and E. Schimmel, "The reticular pattern as a radiographic sign of the Barrett esophagus: an assessment," *Radiology*, Vol.153, pp.333-335, 1984.

[5.5] J. Waring, J. Hunter, M. Oddsdottir, J. Wo, E. Katz, "The preoperative evaluation of patients considered for laparoscopic antireflux surgery," *Am J Gastroenterol.*, Vol.90(1), pp.35-38, 1995.

[5.6] H. Mattox III and J. Richter, "Prolonged ambulatory esophageal pH monitoring in the evaluation of gastroesophageal reflux disease," *The American Journal of Medicine*, Vol.89(3), pp.345-356, 1990.

[5.7] K. DeVault and D. Castell, "Updated guidelines for diagnosis and treatment for gastroesophageal reflux disease," *Am J Gastroenterol.*, Vol.100(1), pp.190-200, 2005.

[5.8] O. Kawamura, M. Aslam, T. Rittmann, C. Hofmann and R. Shaker, "Physical and pH properties of gastroesopharyngeal refluxate: A 24-hour simultaneous Ambulatory Impedance and pH monitoring study," *.Am J Gastroenterol.*, Vol.99(6), pp.1000-1010, 2004.

[5.9] D. Castell and M. Vela, "Combined multichannel intraluminal impedance and pH-metry: an evolving technique to measure type and proximal extent of gastroesophageal reflux," *The American Journal of Medicine*, Vol.11(8), pp.157-159, 2001.

[5.10] R. Tutuian and D. Castell, "Combined multichannel intraluminal impedance and manometry clarifies esophageal function abnormalities: study in 350 patients," *Am J Gastroenterol.*, Vol.99(6), pp.1011-1019, 2004.

[5.11] H. Imam, S. Shay, A. Ali and M. Baker, "Bolus transit patterns in healthy subjects: a study using simultaneous impedance monitoring, videoesophagram, and esophageal manometry," *Am J physiology-GI*, Vol.288(5), pp.1000-1006, 2004.

[5.12] S. Shay, R. Tutuian, D. Sifrim, M. Vela, J. Wise, N. Balaji, X. Zhang, T. Adhami, J. Murray, J. Peters and D. Castell, "Twenty-four hour ambulatory simultaneous impedance and pH monitoring: a multicenter report of normal values from 60 healthy volunteers," *Am J Gastroenterol.*, Vol.99(6), pp.1037-1043, 2004.

[5.13] R. Tutuian, M. Vela, S. Shay and D. Castell, "Multichannel intraluminal impedance in esophageal function testing and gastroesophageal reflux monitoring," *J Clin Gastroenterol*., Vol.37(3), pp.206-215, 2004.

[5.14] Al-Zaben and V. Chandrasekar, “Effect of esophagus status and catheter configuration on multiple intraluminal impedance measurements,” *Physiol. Meas.*, Vol.26(3), pp.229-238, 2005.

[5.15] J. Pandolfino, J. Richter, T. Ours, J. Guardino, J. Chapman and P. Kahrilas, “Ambulatory esophageal pH monitoring using a wireless system,” *Am J Gastroenterol.*, Vol.98(4), pp.740-749, 2003.

[6.1] F. Miranda, R. Simons, and D. Hall, “Validation of radio frequency telemetry concept in the presence of biological tissue-like stratified media,” *IEEE Antennas and Propagation Society International Symposium*, Vol.2, pp.1335-1338, 2004.

[6.2] K.-H. Shin, C.-Y. Moon, T.-H. Lee, C.-H. Lim and Y.-J. Kim, “Implantable flexible wireless pressure sensor module,” *IEEE Sensors*, Vol.2, pp.844-847, 2004.

[6.3] F. Zhu, E. Leonard and N. Levin, “Body composition modeling in the calf using an equivalent circuit model of multi-frequency bioimpedance analysis,” *Physiol. Meas.*, Vol.26(2), pp.S133-S143, 2005.

[6.4] J. Pandolfino, J. Richter, T. Ours, J. Guardino, J. Chapman and P. Kahrilas, “Ambulatory esophageal pH monitoring using a wireless system,” *Am J Gastroenterol.*, Vol.98(4), pp.740-749, 2003.

[6.5] S. Shay, R. Tutuian, D. Sifrim, M. Vela, J. Wise, N. Balaji, X. Zhang, T. Adhami, J. Murray, J. Peters and D. Castell, “Twenty-four hour ambulatory simultaneous impedance and pH monitoring: a multicenter report of normal values from 60 healthy volunteers,” *Am J Gastroenterol.*, Vol.99(6), pp.1037-1043, 2004.

[6.6] K. Wise, D. Anderson, J. Hetke, D. Kipke and K. Najafi, "Wireless implantable microsystems: high-density electronic interfaces to the nervous system," *Proceedings of the IEEE*, Vol.92(1), pp.76-97, 2004.

[6.7] H. Greenhouse, "Design of Planar Rectangular Microelectronic Inductors," *IEEE Transactions on Parts, Hybrids, and Packaging*, Vol.10(2), pp.101-109, 1974.

[6.8] S. Mohan, M. Hershenson, S. Boyd and T. Lee, "Simple accurate expressions for planar spiral inductances," *IEEE Journal of Solid-State Circuits*, Vol.34(10), pp.1419-1424, 1999.

[6.9] Y. Yoon and M. Allen, "Embedded conductor technology for micromachined RF elements," *J. Micromech. Microeng.*, Vol.15, pp.1317-1326, 2005.

[6.10] C. Ahn and M. Allen, "A planar micromachined spiral inductor for integrated magnetic microactuator applications," *J. Micromech. Microeng.*, Vol.3, pp.37-44, 1993.

[6.11] N. Chomnawang, *Three-dimensional micromachined on-chip inductors for high frequency applications*, Ph.D. dissertation, Louisiana State University, 2002.

[7.1] Y. Lee and P. Sorrells, Passive RFID basics, Application Note AN680, Microchip Technology Inc., 2001.

[7.2] M. Ghovanloo and K. Najafi, "A fully digital frequency shift keying demodulator chip for wireless biomedical implants," *IEEE Southwest Symposium on Mixed-Signal Design 2003*, pp.223–227, 2003.

[7.3] K. Finkenzeller, RFID handbook: fundamentals and applications in contactless smart cards and identification, Chichester, England, New York: Wiley; 2003.

[7.4] S. Chen and V. Thomas, "Optimization of inductive RFID technology," *IEEE International Symposium on Electronics and the Environment*, pp.82-87, 2001.

[7.5] G. Vita and G. Iannaccone, "Design criteria for the RF section of UHF and microwave passive RFID transponders," *IEEE Transactions on Microwave Theory and Techniques*, Vol.53(9), pp.2978-2990, 2005.

[7.6] Y. Yao, S. Yin and F. Dai, "A novel low-power input-independent MOS AC/DC charge pump," *IEEE International Symposium on Circuits and Systems*, Vol.1, pp.380-383, 2005.

[7.7] E. Haile and J. Lepkowski, Oscillator Circuits for RTD Temperature Sensors, Application note AN895, Microchip Technology Inc., 2004.

[7.8] microID® 125 kHz RFID System Design Guide, Microchip Technology Inc., 2004.

[7.9] microID® 13.56MHz RFID System Design Guide, Microchip Technology Inc., 2004.

[7.10] K. Wise, D. Anderson, J. Hetke, D. Kipke, K. Najafi, "Wireless implantable microsystems: high-density electronic interfaces to the nervous system," *Proc. IEEE*, Vol.92(1), pp.76-97, 2004.

[7.11] P. R. Troyk and G. A. DeMichele, "Inductively-coupled power and data link for neural prostheses using a class-E oscillator and FSK modulation," *IEEE International Conference Engineering in Medicine and Biology Society*, Vol.4, pp.3376-3379, 2003.

[7.12] N. Chaimanonart, D.J. Young, "Remote RF powering system for wireless MEMS strain sensors," *IEEE Sensors Journal*, Vol.6(2), pp. 484-489, 2006.

[7.13] 2005 IEEE Standard for Safety Levels with Respect to Human Exposure to Radio Frequency Electromagnetic Fields, 3 kHz to 300 GHz, IEEE Std C95.1, 2006.

[7.14] P. Troyk, and M. Schwan, "Closed-loop class E transcutaneous power and data link for microimplants," *IEEE Transactions on Biomedical Engineering*, Vol.39(6), pp.589-599, 1992.

[7.15] P. Sorrells, "Optimizing read range in RFID systems," *Electronics Design, Strategy, News (EDN)*, pp.173-184, Dec 7, 2000.

[7.16] J. Pandolfino, J. Richter, T. Ours, J. Guardino, J. Chapman and P. Kahrilas, "Ambulatory esophageal pH monitoring using a wireless system," *Am J Gastroenterol.*, Vol.98(4), pp.740-749, 2003.

[8.1] E. Haile and J. Lepkowski, Oscillator Circuits for RTD Temperature Sensors, Application note AN895, Microchip Technology Inc., 2004.

[8.2] W.-D. Huang, J. Wang, T. Ativanichayaphong and J.C. Chiao, "Development of an IrOx micro pH sensor array on flexible polymer substrate," *SPIE Smart Structures and Materials & Nondestructive Evaluation and Health Monitoring 2008*, to be published.

BIOGRAPHICAL INFORMATION

Thermpon Ativanichayaphong received his BEEE degree from Chulalongkorn University, Bangkok, Thailand in 1998. He worked at Power Electronics of MINEBEA for 3 years as a production engineer in Hybrid IC division. In 2004, he received his MSEE degree from the University of Texas at Arlington. He received his PhD. in Electrical Engineering from the same school in 2007. During the PhD. study, he has authored and coauthored more than 20 technical publications. His research interests include microelectronics, MEMS, RFIC, RFID, wireless communications and wireless implantable systems.